



Contents lists available at ScienceDirect



# Thermodynamic modeling of CO<sub>2</sub> absorption in aqueous solutions of N,N-diethylethanolamine (DEEA) and N-methyl-1,3-propanediamine (MAPA) and their mixtures for carbon capture process simulation

Seloua Mouhoubi<sup>a</sup>, Lionel Dubois<sup>a</sup>, Philip Loldrup Fosbøl<sup>c</sup>, Guy De Weireld<sup>b</sup>, Diane Thomas<sup>a,\*</sup>

<sup>a</sup> Chemical and Biochemical Process Engineering Unit, University of Mons, 20 Place du Parc, 7000 Mons, Belgium

<sup>b</sup> Thermodynamics Unit, University of Mons, 20 Place du Parc, 7000 Mons, Belgium

<sup>c</sup> Department of Chemical and Biochemical Engineering, Technical University of Denmark, Søltofts Plads Building 229, DK-2800 Kongens Lyngby, Denmark

## ARTICLE INFO

### Article history:

Received 27 June 2019

Received in revised form 24 January 2020

Accepted 25 February 2020

Available online 4 March 2020

### Keywords:

Post-combustion CO<sub>2</sub> capture  
eNRTL thermodynamic modeling  
DEEA-H<sub>2</sub>O-CO<sub>2</sub> system  
MAPA-H<sub>2</sub>O-CO<sub>2</sub> system  
DEEA-MAPA-H<sub>2</sub>O-CO<sub>2</sub> system  
Demixing solvents

## ABSTRACT

Carbone capture by absorption-regeneration technology is a well-known process. However, the development and utilization of new solvents remains crucial to lower its energy consumption. Therefore, an accurate thermodynamic modeling is essential for the process simulation and optimization. This work focuses on the thermodynamic modeling of CO<sub>2</sub> absorption in aqueous solutions of N,N-diethylethanolamine (DEEA), N-methyl-1,3-propanediamine (MAPA) and their mixtures using electrolyte NRTL model. A novel thermodynamic modeling of DEEA-H<sub>2</sub>O-CO<sub>2</sub>, MAPA-H<sub>2</sub>O-CO<sub>2</sub> and DEEA-MAPA-H<sub>2</sub>O-CO<sub>2</sub> systems was developed. The modeling was carried out by considering the pure vapor pressures, excess enthalpies, dielectric constants, physical solubilities of CO<sub>2</sub>, partial and total pressures experimental data. The predicted and correlated data such as vapor-liquid equilibrium (VLE) and heat of CO<sub>2</sub> absorption were compared favorably to experimental data from the literature. Liquid-liquid phase separation of a specific mixture of these two amines was also highlighted. Subsequently, the developed model could be used for further simulations at large scale considering that successful validation was performed at pilot scale.

© 2020 Institution of Chemical Engineers. Published by Elsevier B.V. All rights reserved.

## 1. Introduction

The global warming has become a serious environmental concern over these last decades. Nowadays, as carbon dioxide is the most important source of anthropogenic greenhouse gases emissions, reduction of CO<sub>2</sub> emissions is a key point for climate change mitigation. In order to reduce CO<sub>2</sub> emissions from the industrial sector, a combination of solutions such as reduction of energy consumption, improvement of energy efficiency, development of renewable energies and implemen-

tation of CO<sub>2</sub> capture and utilization or storage (CCUS) technologies are necessary.

The most advanced and mature carbon capture technology is the post-combustion CO<sub>2</sub> capture using absorption-regeneration process with amine-based solvents. In the last decade, many CO<sub>2</sub> post-combustion pilots and demonstration plants have been built and were operated ([Idem et al., 2015](#)). Nevertheless, absorption-regeneration process with amine-based solvents involves a high energy consumption, mainly related to the solvent regeneration. In order to improve this process and to reduce its costs, different solutions were proposed such as the use of more efficient equipment ([Zhao et al., 2011](#)), the implementation of new process configurations ([Dubois and Thomas, 2018](#)) and the development of new solvents ([Singh et al., 2013](#)). A large variety of

\* Corresponding author.

E-mail address: [diane.thomas@umons.ac.be](mailto:diane.thomas@umons.ac.be) (D. Thomas).

<https://doi.org/10.1016/j.cherd.2020.02.029>

0263-8762/© 2020 Institution of Chemical Engineers. Published by Elsevier B.V. All rights reserved.

## Nomenclature

### Notations

|              |  |
|--------------|--|
| $f$          | Fugacity (kPa)                                   |
| $g^E$        | Excess Gibbs energy (kJ/mol)                     |
| $H$          | Henry's constant (Pa)                            |
| $H^E$        | Excess enthalpy (kJ/mol)                         |
| $K$          | Equilibrium constant                             |
| $p$          | Pressure (Pa)                                    |
| $q$          | Critical volume                                  |
| $R$          | Ideal gas constant (J/mol K)                     |
| $T$          | Temperature (K for equations and °C for figures) |
| $w$          | Liquid mass fraction                             |
| $x$          | Liquid mole fraction                             |
| $y$          | Vapor mole fraction                              |
| $\Delta G^0$ | Standard Gibbs free energy change (kJ/mol)       |

### Greek letters

|               |                                     |
|---------------|-------------------------------------|
| $\alpha_{ij}$ | Non-randomness factor of NRTL model |
| $\gamma$      | Activity coefficient                |
| $\varepsilon$ | Dielectric constant                 |
| $\sigma$      | Standard deviation                  |
| $\tau_{ij}$   | Binary parameter of NRTL model      |
| $\Phi$        | Fugacity coefficients               |
| $\Psi$        | Poynting factor                     |
| $\mu$         | Chemical potential                  |

### Subscripts and exponents

|          |                        |
|----------|------------------------|
| *        | Unsymmetric convention |
| 0        | Pure component         |
| $\infty$ | Infinite dilution      |
| a        | Anion                  |
| c        | Cation                 |
| lc       | Local composition      |
| m        | Molecule               |
| PDH      | Pitzer–Debye–Hückel    |

amine-based solvents for CO<sub>2</sub> capture can be found in the literature. The alkanolamine are divided into three main categories: primary, secondary and tertiary amines. Primary and secondary amines are mainly known for their high reaction rate with CO<sub>2</sub>, whereas tertiary amines provide a high CO<sub>2</sub> absorption capacity (Khan et al., 2016; Xiao et al., 2018). Compared to tertiary amines, primary and secondary amines require higher energy regeneration due to carbamate formation. Consequently, blending the two amine types can allow to take advantage from the best properties of each amine in the mixture (Du et al., 2016; Brüder et al., 2012).

Among amine mixtures used for CO<sub>2</sub> capture, an innovative blend of N,N-diethylethanolamine (DEEA), a tertiary amine and N-methyl-1,3-propanediamine (MAPA), a diamine with a primary and a secondary amino group, has been drawing a particular attention (Pinto et al., 2014a; Monteiro et al., 2015b; Arshad et al., 2016; Pinto et al., 2017; Perinu et al., 2018; Garcia et al., 2018). Indeed, this mixture is characterized by its high reaction rate, absorption capacity and cyclic capacity with high CO<sub>2</sub> pressure in the stripping column (Pinto et al., 2014b; Bernhardsen et al., 2018). Moreover, under certain conditions of concentration and CO<sub>2</sub> loading, this system can split into two liquid phases, one rich and one lean in CO<sub>2</sub>. This phenomenon can potentially allow an important energy saving by regenerating only the CO<sub>2</sub>-rich phase after a separation in a decanter unit, the CO<sub>2</sub>-lean phase being recycled back directly to the absorber (Liebenthal et al., 2013; Raynal et al., 2011).

When CO<sub>2</sub> is dissolved in aqueous amine solutions, it forms electrolytes. The more versatile models used for thermodynamic modeling of electrolyte systems containing H<sub>2</sub>O-amine-acid gas are electrolyte NRTL (Chen et al., 1982) (non-random two liquid) or Extended UNI-

QUAC (Sander et al., 1986) (universal quasi-chemical). Electrolyte NRTL model has been successfully used for a large variety of H<sub>2</sub>O-amine-acid systems. Among these studies, mention may be made of le Bouhelec et al. (2007) who implemented eNRTL model to determine interaction parameters using VLE and heat of absorption data for MEA-H<sub>2</sub>O-CO<sub>2</sub>, DEA-H<sub>2</sub>O-CO<sub>2</sub> and MDEA-H<sub>2</sub>O-CO<sub>2</sub> systems. Electrolyte NRTL model has been also used by Mondal et al. (2015) for the modeling of the CO<sub>2</sub> solubility in aqueous solutions of hexamethylenediamine (HMDA). Li et al. (2015) has also implemented this model to study 1-methylpiperazine-H<sub>2</sub>O-CO<sub>2</sub> system.

Vapor-liquid thermodynamic modeling of DEEA-H<sub>2</sub>O-CO<sub>2</sub> system was carried out by some authors (Monteiro et al., 2013; Xu et al., 2014); and recently Garcia et al. (2016) using eNRTL model. Nevertheless, the implementation of the proposed interaction parameters in Aspen Plus™ (V10) does not give a suitable representation of the vapor-liquid equilibrium experimental data. Arshad et al. (2016) studied the thermodynamic of DEEA-H<sub>2</sub>O-CO<sub>2</sub>, MAPA-H<sub>2</sub>O-CO<sub>2</sub> and their mixture with Extended UNIQUAC thermodynamic model using an in-house tool. However, no thermodynamic modeling study was found in the literature for the loaded aqueous MAPA solutions and DEEA-MAPA mixtures using eNRTL model. Therefore, in this work, a complete modeling of DEEA-H<sub>2</sub>O-CO<sub>2</sub>, MAPA-H<sub>2</sub>O-CO<sub>2</sub> and DEEA-MAPA-H<sub>2</sub>O-CO<sub>2</sub> systems using eNRTL model is presented.

This work focuses on the study of DEEA-MAPA-H<sub>2</sub>O mixtures for CO<sub>2</sub> capture by developing a thermodynamic model which can be used for absorption-regeneration process simulation. First, an accurate and comprehensive thermodynamic modeling using Aspen Plus™ (V10) tool was developed for the two subsystems DEEA-H<sub>2</sub>O-CO<sub>2</sub> and MAPA-H<sub>2</sub>O-CO<sub>2</sub> separately. Then, additional parameters were regressed in order to consider the interactions of the global DEEA-MAPA-H<sub>2</sub>O-CO<sub>2</sub> system. Finally, a validation of the process modeling by absorption-regeneration at pilot scale (including kinetic considerations, viscosity and density modeling) was performed.

## 2. Thermodynamic modeling description

### 2.1. Electrolyte NRTL model

The electrolyte NRTL model states that the excess Gibbs energy of a solvent is expressed as the sum of three contributions (Eq. (1)). The first contribution is the short-range term which is related to the local ion-molecule, ion-ion, and molecule-molecule interactions that exist in the immediate neighborhood of any species. The second term is related to the long-range ion-ion interactions that exist beyond the immediate neighborhood of a central ionic species. The long-range term is represented by the Pitzer–Debye–Hückel term, and the third contribution concerns the Born term used for the infinite dilution aqueous reference state.

$$\frac{g^{E^*}}{RT} = \frac{g^{E^*,lc}}{RT} + \frac{g^{E^*,PDH}}{RT} + \frac{g^{E^*,Born}}{RT} \quad (1)$$

There are no adjustable parameters related to the long-range ion-ion interaction contribution. However, for the short-range term, adjustable asymmetric binary parameters,  $\tau_{ij}$ , and symmetric non-randomness factor,  $\alpha_{ij}$ , are required. There are two interaction parameters for each molecule-molecule, ion-molecule and ion-ion pair. The probability of ion-ion pair interactions being very low in the studied system, this interaction has been neglected and defaulted to zero as in Zhang and Chen (2011). The simplified temperature dependency of the remaining interaction parameters is expressed as follows (Eqs. (2)–(4)):

- Molecule-molecule binary parameters

**Table 1 – Chemical equilibrium equations and constants.**

| Equation  | $\ln K_j(T = 40^\circ\text{C})$ | Number |
|---|---------------------------------|--------|
| $2\text{H}_2\text{O} \leftrightarrow \text{H}_3\text{O}^+ + \text{OH}^-$                              | -39.24                          | (5)    |
| $2\text{H}_2\text{O} + \text{CO}_2 \leftrightarrow \text{H}_3\text{O}^+ + \text{HCO}_3^-$             | -18.68                          | (6)    |
| $\text{HCO}_3^- + \text{H}_2\text{O} \leftrightarrow \text{H}_3\text{O}^+ + \text{CO}_3^{2-}$         | -27.55                          | (7)    |
| $\text{DEEAH}^+ + \text{H}_2\text{O} \leftrightarrow \text{DEEA} + \text{H}_3\text{O}^+$              | -24.79                          | (8)    |
| $\text{MAPAH}^+ + \text{H}_2\text{O} \leftrightarrow \text{MAPA} + \text{H}_3\text{O}^+$              | -29.46                          | (9)    |
| $\text{H}^+\text{MAPAH}^+ + \text{H}_2\text{O} \leftrightarrow \text{MAPAH}^+ + \text{H}_3\text{O}^+$ | -23.02                          | (10)   |
| $\text{MAPA} + \text{HCO}_3^- \leftrightarrow \text{MAPACOO}^- + \text{H}_2\text{O}$                  | 12.77                           | (11)   |

$$\tau_{mm'} = A_{mm'} + \frac{B_{mm'}}{T} \quad (2)$$

- Cation (or anion)–molecule pair parameters

$$\tau_{ca,m} = A_{ca,m} + \frac{B_{ca,m}}{T} \quad (3)$$

- Molecule–cation (or anion) pair parameters

$$\tau_{m,ca} = A_{m,ca} + \frac{B_{m,ca}}{T} \quad (4)$$

Two different reference states for the molecules and ions are used. For molecular species, the pure liquid state at the same temperature is used as a reference state, and for ionic species, the infinite-dilution aqueous solution reference state is used (Prausnitz et al., 1999). For more information, details on electrolyte model are available in the literature (Chen and Evans, 1986; Austgen et al., 1989).

## 2.2. Chemical equilibrium

Depending on the amine type, several reactions take place when carbon dioxide is solubilized in aqueous amine solutions. The reactions presented in Table 1 are commonly considered to describe the chemical equilibrium in DEEA–H<sub>2</sub>O–CO<sub>2</sub>, MAPA–H<sub>2</sub>O–CO<sub>2</sub> system and their mixtures (Arshad et al., 2016; Monteiro et al., 2013). Perinu et al. (2019) have identified from the NMR study of MAPA system: MAPA(aq), protonated MAPA (MAPAH<sup>+</sup>), di-protonated MAPA (H<sup>+</sup>MAPAH<sup>+</sup>), primary MAPA carbamates/protonated primary carbamates (MAPACOO<sup>−</sup>(p)/MAPAH<sup>+</sup>COO<sup>−</sup>(p)), secondary MAPA carbamates/protonated secondary carbamates (MAPACOO<sup>−</sup>(s)/MAPAH<sup>+</sup>COO<sup>−</sup>(s)) and dicarbamates (MAPA(COO<sup>−</sup>)<sub>2</sub>). However, as considered in (Arshad et al., 2016), the formation of secondary carbamates and dicarbamates is very small and the primary carbamates of MAPA are the dominating carbamate species present in the aqueous phase. Hence, four species of MAPA; MAPA(aq), MAPAH<sup>+</sup>, H<sup>+</sup>MAPAH<sup>+</sup> and primary MAPA carbamates MAPACOO<sup>−</sup> were considered for the modeling as shown in Table 1.

In the considered system, DEEAH<sup>+</sup>, MAPAH<sup>+</sup>, H<sup>+</sup>MAPAH<sup>+</sup> and MAPACOO<sup>−</sup> species were not defined in Aspen Plus<sup>TM</sup> database. To define these species, the molecular weight, free energy of formation and enthalpy of formation were retrieved from Arshad et al. (2016).

The equilibrium reaction constants are calculated from the standard Gibbs free energy (Eqs. (5)–(11)) using the following equation (Eq. (12)):

$$K_j = \exp \left( -\frac{\Delta G_j^0(T)}{RT} \right) \quad (12)$$

**Table 2 – Pure physical properties of H<sub>2</sub>O, DEEA, MAPA and CO<sub>2</sub>.**

| Parameter                             | H <sub>2</sub> O | DEEA   | MAPA    | CO <sub>2</sub> |
|---------------------------------------|------------------|--------|---------|-----------------|
| T <sub>C</sub> (K)                    | 647.096          | 592    | 599     | 304.21          |
| P <sub>C</sub> (kPa)                  | 22,064           | 3180   | 4693.64 | 73,383          |
| V <sub>C</sub> (m <sup>3</sup> /kmol) | 0.05595          | 0.401  | 0.3277  | 0.094           |
| Z <sub>C</sub>                        | 0.229            | 0.259  | 0.309   | 0.274           |
| Acentric factor                       | 0.3445           | 0.7817 | 0.5711  | 0.2236          |

where R is the ideal gas constant, T is the temperature and  $\Delta G_j^0(T)$  is the standard reaction Gibbs energy change.

The critical parameters as well as the acentric factor and compressibility factor of H<sub>2</sub>O, DEEA, MAPA and CO<sub>2</sub> are listed in Table 2.

## 2.3. Vapor–liquid equilibrium

Chemical equilibrium results in equal chemical potentials for each component in each phase as follows:

$$\mu_i^{vap}(T, p, y) = \mu_i^{liq}(T, p, x) \quad (13)$$

where  $\mu_i^{vap}$  and  $\mu_i^{liq}$  are the chemical potentials of the species i in the vapor and liquid phases, respectively.

In this case, an activity solution model is used for the liquid phase (eNRTL) and an equation of state for the vapor phase (Redlich–Kwong equation of state). The vapor–liquid equilibrium (Eq. (13)) is expressed as follows (Eqs. (14)–(15)) (Austgen et al., 1989):

- For components at pure reference state

$$p y_i \Phi_i = x_i \gamma_i p_i^0 \phi_i^0 \psi_i \quad (14)$$

where p is the pressure of the system,  $\gamma_i$  and  $\Phi_i$  are the activity and fugacity coefficients of the species i.  $y_i$  and  $x_i$  are respectively the vapor and liquid mol fraction of a component i.  $p_i^0$  is the pure vapor pressure and  $\phi_i^0$  is the pure fugacity coefficients at  $p_i^0$ .  $\psi_i$  is the pressure correction factor (Poynting factor).

- For components at infinite dilution reference state

$$p y_i \Phi_i = x_i \gamma_i^* H_i^\infty \psi_i \quad (15)$$

where  $H_i^\infty$  is the Henry's constant at infinite dilution reference state, and  $\gamma_i^*$  is the unsymmetrical activity coefficient.

## 2.4. Data regressions and parameter settings

Thermodynamic modeling is essential for a good prediction of the vapor–liquid equilibria, the heat of CO<sub>2</sub> absorption and the solution speciation. In the present work, model parameters were estimated for DEEA–H<sub>2</sub>O–CO<sub>2</sub>, MAPA–H<sub>2</sub>O–CO<sub>2</sub> and their mixture by using a variety of available experimental data: pure amine vapor pressure (Hartono et al., 2013; Kim et al., 2008), DEEA excess enthalpy (Mathonat et al., 1997), binary DEEA–H<sub>2</sub>O and binary DEEA–MAPA vapor–liquid equilibrium (VLE) (Hartono et al., 2013). The vapor–liquid equilibrium data of CO<sub>2</sub> absorption in aqueous solutions of DEEA, MAPA and their mixtures were retrieved from Arshad et al. (2014) and Monteiro et al. (2013).

The regressions were carried out using Aspen Plus<sup>TM</sup> (V10) data regression tool (DRS) with Britt–Luecke algorithm using

the maximum likelihood minimization objective function. The deviation between the model results and the experimental data is expressed (Eq. (16)) as an absolute average relative deviation (AARD):

$$AARD = \frac{1}{N} \sum_N \left| \frac{\varphi_{calc} - \varphi_{exp}}{\varphi_{exp}} \right| \times 100 \quad (16)$$

where  $N$  is the number of points considered,  $\varphi$  is the type of data. “calc” represents the calculated data using the model and “exp” the experimental points.

Pure amine vapor pressure parameters were regressed for pure DEEA and MAPA using Extended Antoine model defined by Eq. (17):

$$\ln(p_i^0) = A_i + \frac{B_i}{T} + C_i \ln(T) + D_i T^{E_i} \quad (17)$$

The dielectric constants of pure DEEA and MAPA were not available in the literature. Therefore, thanks to similarities in amines structures, the constant of pure DEEA (Eq. (18)) was assumed to be equal to that of MDEA (*N*-methylidiethanolamine) (Dash and Bandyopadhyay, 2016). In the case of pure MAPA, the dielectric constant (Eq. (19)) was assumed to be equal to that of *N,N'*-bis(2aminoethyl)-1,2-ethandiamine (Lide, 2005).

$$\varepsilon_{DEEA}(T) = 21.9957 + 8992.68 \left( \frac{1}{T} - \frac{1}{298.15} \right) \quad (18)$$

$$\varepsilon_{MAPA}(T) = 10.45 + 4411.8 \left( \frac{1}{T} - \frac{1}{298.15} \right) \quad (19)$$

A mixing rule (Eq. (20)) is used to calculate the dielectric constant of mixed solvent by mass averaging the pure solvent dielectric constants as follows:

$$\varepsilon_{mixture}(T) = \sum_i w_i \varepsilon_i(T) \quad (20)$$

The dielectric constants of aqueous solutions of DEEA and MAPA were calculated using the mixing rule and compared to experimental data from Monteiro and Svendsen (2015) as shown in Supplementary Information (Fig. SI.1). The calculated results are in good agreement with experimental data for DEEA at 2 M and 5 M and for 2 M MAPA.

Henry's constant allows to quantify the physical solubility of a compound in a solvent. Usually, the N<sub>2</sub>O analogy is applied to determine the CO<sub>2</sub> solubility in amine solutions. Nevertheless, it is important to note that the use of N<sub>2</sub>O analogy may be restricted to systems that are much more dilute than what is of industrial interest, for example 5 M MEA (Monteiro and Svendsen, 2015). However, because of the lack of rigorous models for determining the CO<sub>2</sub> solubility in amine solutions, the N<sub>2</sub>O analogy is mainly applied.

The gas solubility can be estimated in mixed solvents by providing the solubility of the gas in each of the pure solvent constituting the mixture. A mixing rule was used to calculate Henry's constant into aqueous amine solutions from the Henry's constant in pure amine and the Henry's constant in pure water (Prausnitz et al., 1999). The expression used to cal-

culate Henry's constant of a solute in a mixture is given by Eq. (21).

$$\ln(H_{CO_2,mixture}) = \sum_i Z_i \ln(H_{CO_2,i}) \quad (21)$$

$$Z_i = \frac{x_i q_i^{2/3}}{\sum_i x_i q_i^{2/3}} \quad (22)$$

where  $H_{CO_2,i}$  is Henry's constant of CO<sub>2</sub> in pure solvent  $i$ ,  $Z_i$  (Eq. (22)) is the weighting factor,  $x_i$  is the solvent mole fraction and  $q_i$  is the critical volume of each solvent (Zhang and Chen, 2011).

The Henry's constant parameters as function of temperature in pure amine were regressed using N<sub>2</sub>O analogy. Experimental results of N<sub>2</sub>O Henry's constant ( $H_{N_2O,DEEA}$ ) were retrieved from Monteiro et al. (2015a) and different values of the ratio  $H_{CO_2,H_2O}/H_{N_2O,H_2O}$  as function of the temperature retrieved from Ma'mun and Svendsen (2009). The expression of Henry's constant in pure DEEA and MAPA is given as follows (Eqs. (23)-(24)):

$$\ln(H_{CO_2,DEEA}) = 18.648 - \frac{936.09}{T} \quad (23)$$

$$\ln(H_{CO_2,MAPA}) = 13.839 - \frac{1289.5}{T} \quad (24)$$

Binary molecule–molecule interaction parameters and cation (or anion)–molecule pair parameters were also regressed. In the case of cation (or anion)–molecule pair parameters regression the default values were set to:  $A_{CO_2,ca} = 15$ ,  $A_{ca,CO_2} = -8$ ,  $A_{amine,ca} = 8$ ,  $A_{ca,amine} = -4$ ,  $A_{H_2O,ca} = 8$  and  $A_{ca,H_2O} = -4$  as in Aspen Plus<sup>TM</sup>, based on typical eNRTL values from Chen et al. (1982). The cation (or anion)–anion (or cation) parameters are defaulted to zero. The non-randomness parameters were set to 0.2 for water–salt pairs and 0.1 for Amine/CO<sub>2</sub>–salt pairs, as in Hessen et al. (2010) and Chen and Rochelle (2013).

The experimental data used for the regression of the different model parameters and for the validation of the developed model are summarized in Appendix A.

### 3. Results and discussion

#### 3.1. Amine pure vapor pressure

The pure amine vapor pressures were regressed using experimental data of Hartono et al. (2013) from 64 to 160 °C for DEEA, and experimental data of Kim et al. (2008) and Hartono et al. (2013) from 54 to 140 °C for MAPA as shown in Fig. 1. The results are expressed using extended Antoine equation model (Eq. (17)). For pure water a correlation from Daubert et al. (1993) was used and compared to experimental results from Kim et al. (2008) and Trolleøa et al. (2013). The water and pure amines vapor pressures were therefore expressed by Eqs. (25)–(27):

$$\ln(p_{H_2O}^0) = 73.649 - \frac{7258.2}{T} - 7.3037 \ln(T) - 4.1653^{-6} T^2 \quad (25)$$

$$\begin{aligned} \ln(p_{DEEA}^0) = 65.605 & - \frac{7786.61}{T} - 5.9357 \ln(T) \\ & - 1.9777^{-16} T^{5.0733} \end{aligned} \quad (26)$$

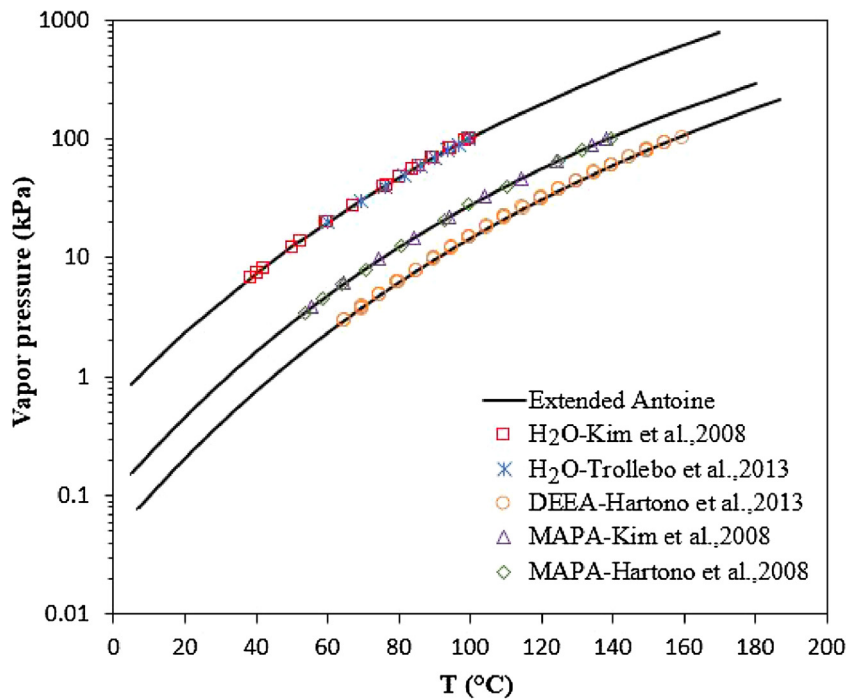


Fig. 1 – Pure  $\text{H}_2\text{O}$ , DEEA and MAPA vapor pressures as function of temperature.

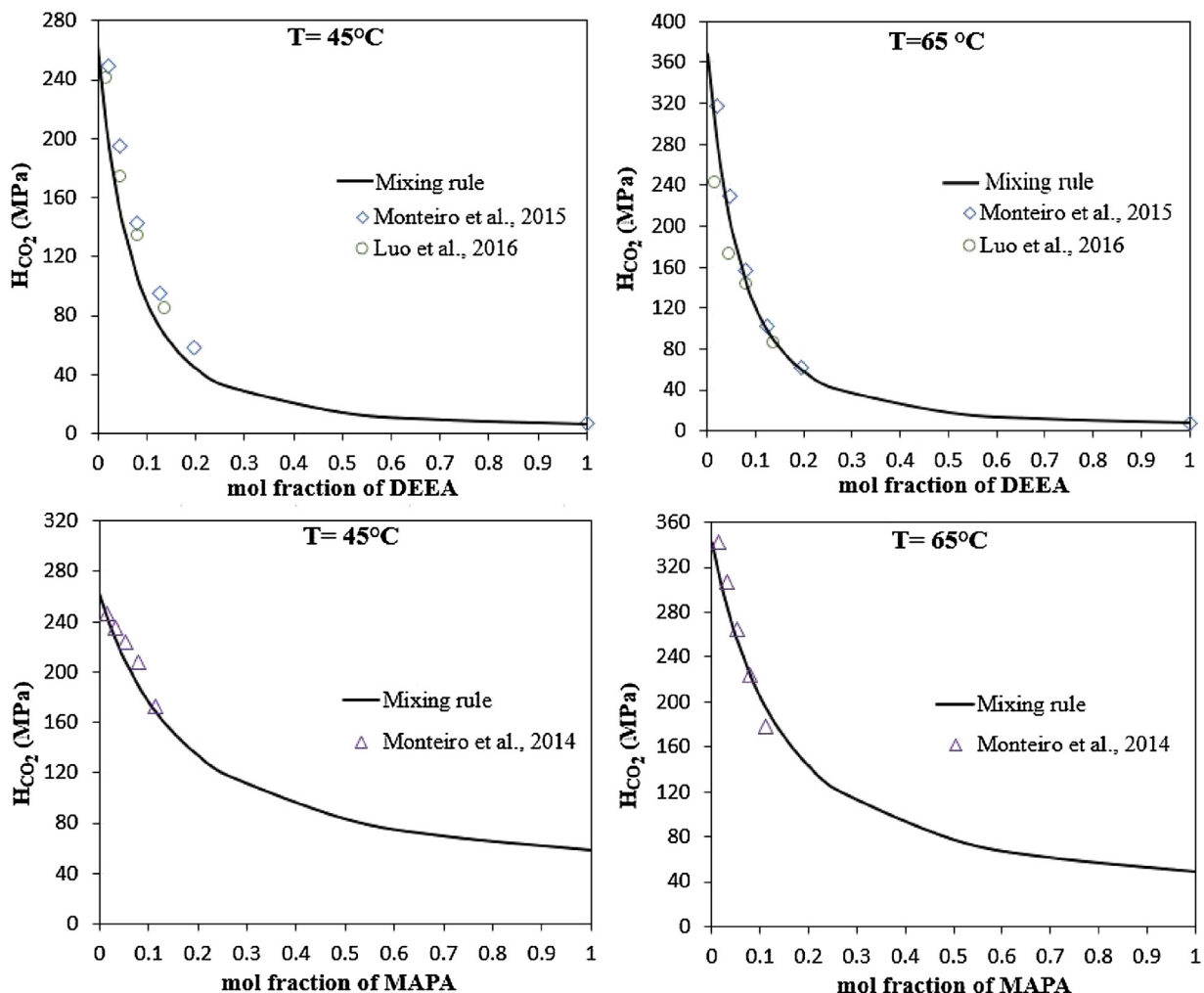


Fig. 2 – Henry's constants of  $\text{CO}_2$  into aqueous solutions of DEEA (top) and MAPA (bottom) as function of amine composition at 45 °C (left) and 65 °C (right).

**Table 3 – Regression results of DEEA-H<sub>2</sub>O NRTL binary parameters.**

| Parameter        | Molecule m       | Molecule m'      | Value   |
|------------------|------------------|------------------|---------|
| A <sub>mm'</sub> | DEEA             | H <sub>2</sub> O | 2.7726  |
| A <sub>m'm</sub> | H <sub>2</sub> O | DEEA             | 7.1046  |
| B <sub>mm'</sub> | DEEA             | H <sub>2</sub> O | -960.10 |
| B <sub>m'm</sub> | H <sub>2</sub> O | DEEA             | -1403.5 |
| $\alpha_{mm'}$   | H <sub>2</sub> O | DEEA             | 0.5575  |

$$\ln(p_{MAPA}^0) = 38.936 - \frac{8152.05}{T} - 7.7394 \ln(T) + 38.935 T^{0.00015} \quad (27)$$

The absolute average relative deviation between experimental and calculated results was 1.5% for DEEA, 1% for MAPA and 0.4% for water.

### 3.2. Henry's constant

Fig. 2 shows a comparison between Henry's constant of CO<sub>2</sub> into aqueous solutions of DEEA and MAPA calculated results versus experimental data. It can be seen that the results calculated using the mixing rule match quite well with the experimental data with a relative deviation of 12.66% compared to Monteiro et al. (2015a) results and of 14.62% compared to Luo et al. (2016) results for DEEA solutions. In the case of MAPA solutions, the deviation was 5.12% compared to experimental results from Monteiro et al. (2014).

### 3.3. Electrolyte NRTL parameters regressions

#### 3.3.1. DEEA based system

The binary interaction parameters between DEEA and H<sub>2</sub>O were regressed using binary VLE (TPxy) data at different temperatures (50, 60, 80 and 95 °C) from Hartono et al. (2013) and excess enthalpy data from Mathonat et al. (1997). The results are given in Table 3.

It can be seen from Fig. 3 that the model gives a very good representation of the experimental data with an average deviation of 4.6% for the excess enthalpy (H<sup>E</sup>) compared to experimental results from Mathonat et al. (1997) and of 2.33% for the binary VLE data compared to experimental results from Hartono et al. (2013).

From the vapor-liquid equilibrium plot (Fig. 3) it can be observed that the mixture of DEEA and water exhibits an

**Table 4 – DEEA-H<sub>2</sub>O-CO<sub>2</sub> system cation (or anion)-molecule pair regressed results.**

| Component m/ca  | Component m/ca  | A <sub>m,ca</sub> /A <sub>ca,m</sub> | B <sub>m,ca</sub> /B <sub>ca,m</sub> |
|---|---|--------------------------------------|--------------------------------------|
| H <sub>2</sub> O                                      | (DEEAH <sup>+</sup> , HCO <sub>3</sub> <sup>-</sup> ) | 6.5756                               | -1111.3                              |
| (DEEAH <sup>+</sup> , HCO <sub>3</sub> <sup>-</sup> ) | H <sub>2</sub> O                                      | -6.7220                              | 1127.9                               |
| H <sub>2</sub> O                                      | (DEEAH <sup>+</sup> , CO <sub>3</sub> <sup>2-</sup> ) | 52.617                               | -13,084.9                            |
| (DEEAH <sup>+</sup> , CO <sub>3</sub> <sup>2-</sup> ) | H <sub>2</sub> O                                      | -22.654                              | 5112.7                               |
| DEEA  | (DEEAH <sup>+</sup> , HCO <sub>3</sub> <sup>-</sup> ) | 30.910                               | -7385.9                              |
| (DEEAH <sup>+</sup> , HCO <sub>3</sub> <sup>-</sup> ) | DEEA  | 4.0963                               | -727.28                              |
| DEEA  | (DEEAH <sup>+</sup> , CO <sub>3</sub> <sup>2-</sup> ) | 8.2671                               | -1401.5                              |
| (DEEAH <sup>+</sup> , CO <sub>3</sub> <sup>2-</sup> ) | DEEA  | -20.437                              | 9132.3                               |

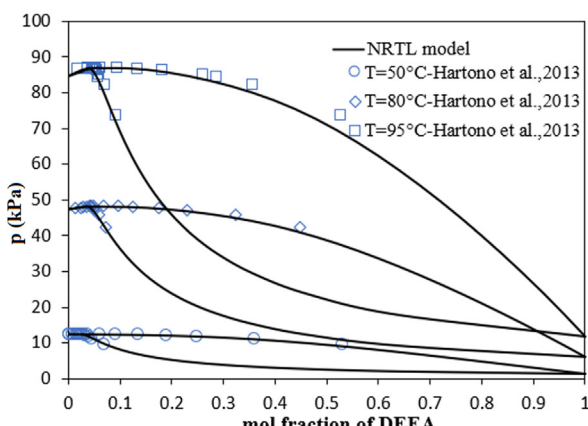
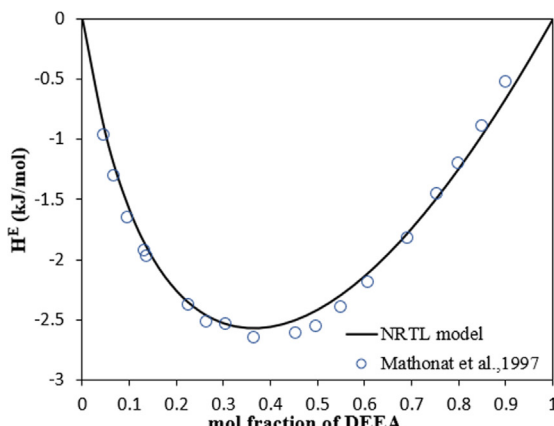
azeotrope at quite low aqueous DEEA concentrations ( $x < 0.1$ ). This azeotrope is correctly represented by the model.

For the regression of cation (or anion)-molecule pair parameters a simplifying assumption was adopted and verified later by assuming that CO<sub>2</sub>(aq), OH<sup>-</sup> and H<sub>3</sub>O<sup>+</sup> are present in low concentrations in the system. Hence, the parameters related to interactions involving one of these species were set to default values, as shown previously. Therefore, 16 cation (or anion)-molecule pair interaction parameters were regressed using experimental VLE data from Arshad et al. (2014) and Monteiro et al. (2013). The regressed parameters are given in Table 4.

The regressed parameters were used to predict the CO<sub>2</sub> loaded amine systems through the fit of the total and partial pressures of CO<sub>2</sub>, the heat of CO<sub>2</sub> absorption and speciation. The CO<sub>2</sub> partial pressure and the total pressure are shown in Fig. 4 as function of the CO<sub>2</sub> loading. It can be seen that the model represents quite well the experimental data for 2 M (23.7 wt%) and 5 M (61.2 wt%) DEEA at 40, 60, 80, 100, and 120 °C. The estimated absolute average relative deviation (AARD) for 2 M DEEA are respectively 5.83% and 9% for the total pressure and CO<sub>2</sub> partial pressure compared to experimental results from Monteiro et al. (2013).

In the case of 5 M DEEA, the estimated AARD are respectively 6.91% and 14.52% for the total pressure and CO<sub>2</sub> partial pressure compared to experimental results from Monteiro et al. (2013), and of respectively 8.62% and 19.63% for the total pressure and CO<sub>2</sub> partial pressure compared to experimental results from Arshad et al. (2014). As the CO<sub>2</sub> partial pressures reported in Arshad et al. (2014) are estimated from the total pressures, only the total pressures have been used in the fitting procedure.

Furthermore, model results of CO<sub>2</sub> partial pressure were compared to experimental data from Xu et al. (2014) and Luo

**Fig. 3 – Excess enthalpy of DEEA solutions (left) and DEEA-H<sub>2</sub>O vapor-liquid equilibrium (right) as function of DEEA mole fraction.**

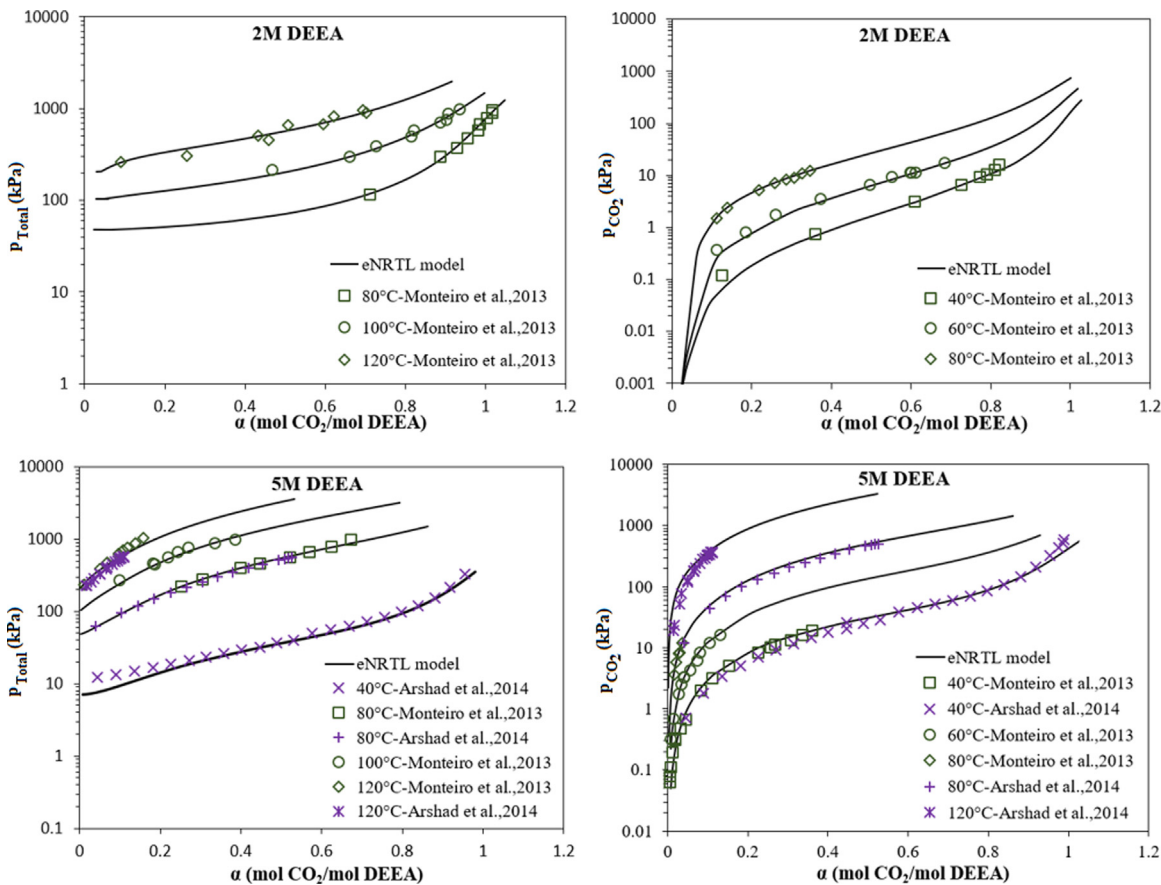


Fig. 4 – Total pressure (left) and  $\text{CO}_2$  partial pressure (right) for 2 M DEEA (top) and 5 M DEEA (bottom) as function of the loading.

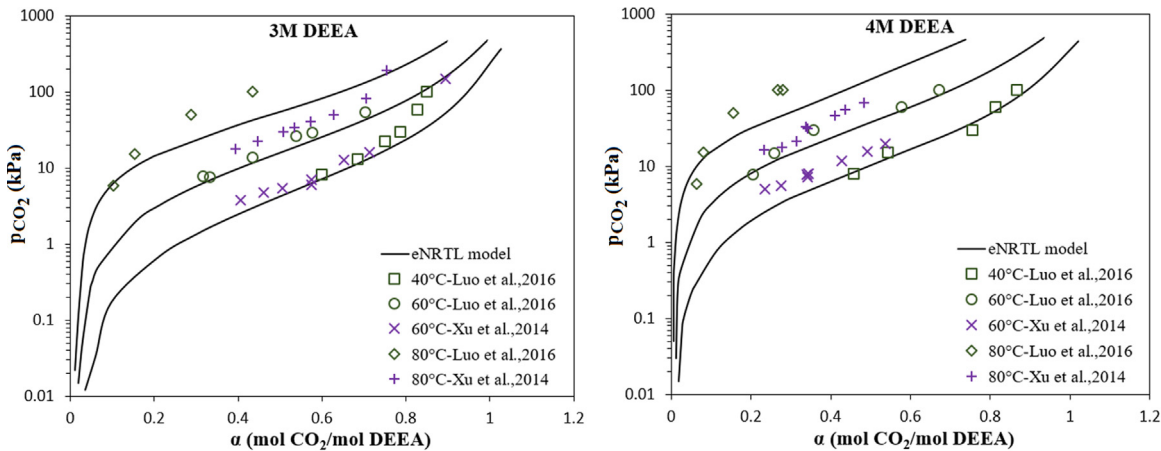


Fig. 5 –  $\text{CO}_2$  partial pressure 3 M DEEA (left) and 4 M DEEA (right) as function of the loading.

et al. (2016) at 3 M (35.8 wt%) and 4 M (48.2 wt%) DEEA. Nevertheless, an important disparity can be observed between the experimental results from the two sources as shown in Fig. 5. The predicted results are almost in between the experimental results from the two literature sources. Unfortunately, there is no information about the experimental errors on measurements in these studies allowing to give more comments.

The predicted speciation results were compared to experimental data from Gifftja et al. (2013) for 2.64 M DEEA (Fig. 6, left) and to experimental data from Perinu et al. (2019) for 3 M DEEA (Fig. 6, right).

Globally, the trends are similar for the two amine concentrations compared to the model predicted results. As the NMR

analysis used in Perinu et al. (2019) does not allow to quantify DEEA and  $\text{DEEAH}^+$  as well as  $\text{HCO}_3^-$  and  $\text{CO}_3^{2-}$  separately, the sum of these species was considered for the modeled results. The total concentration of  $\text{HCO}_3^- + \text{CO}_3^{2-}$  is continuously increasing from the low  $\text{CO}_2$  loadings until 1 mol  $\text{CO}_2/\text{mol DEEA}$ . Indeed, bicarbonates are the main components that can be found during  $\text{CO}_2$  absorption into aqueous solution of tertiary amines such as DEEA. Another product has been identified by Perinu et al. (2019), this species is a tertiary amino carbonate (DEEAOCOO $^-$ ), however it was found in negligible amount as shown in (Fig. 6, right). The detailed predicted speciation including the species separately as function of the  $\text{CO}_2$  loading for 2 M DEEA at 40 °C can be found in Fig. SI.7 in Supplementary Information.

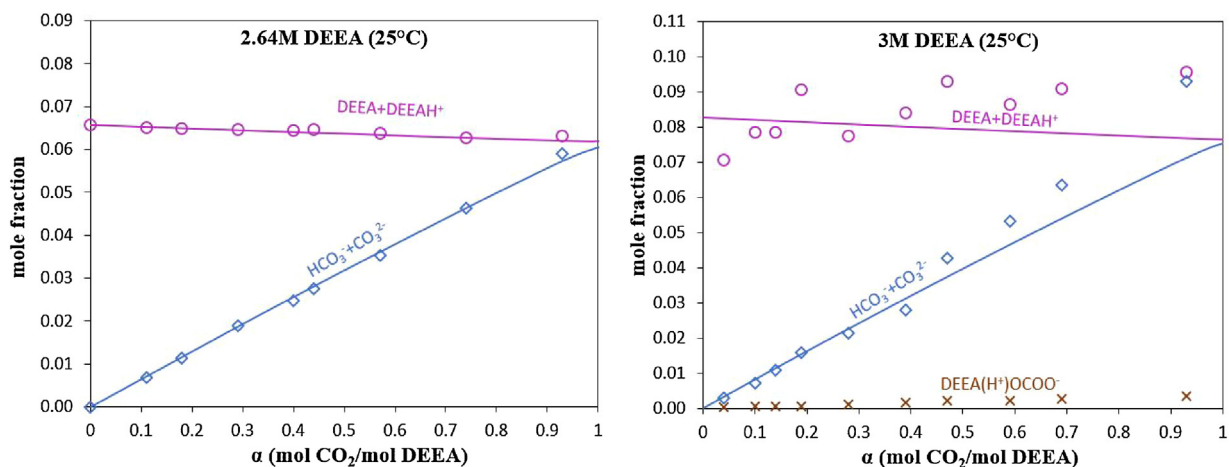


Fig. 6 – Speciation for 2.64 M DEEA (left) and 3 M DEEA (right) at 25 °C, model results (solid lines).

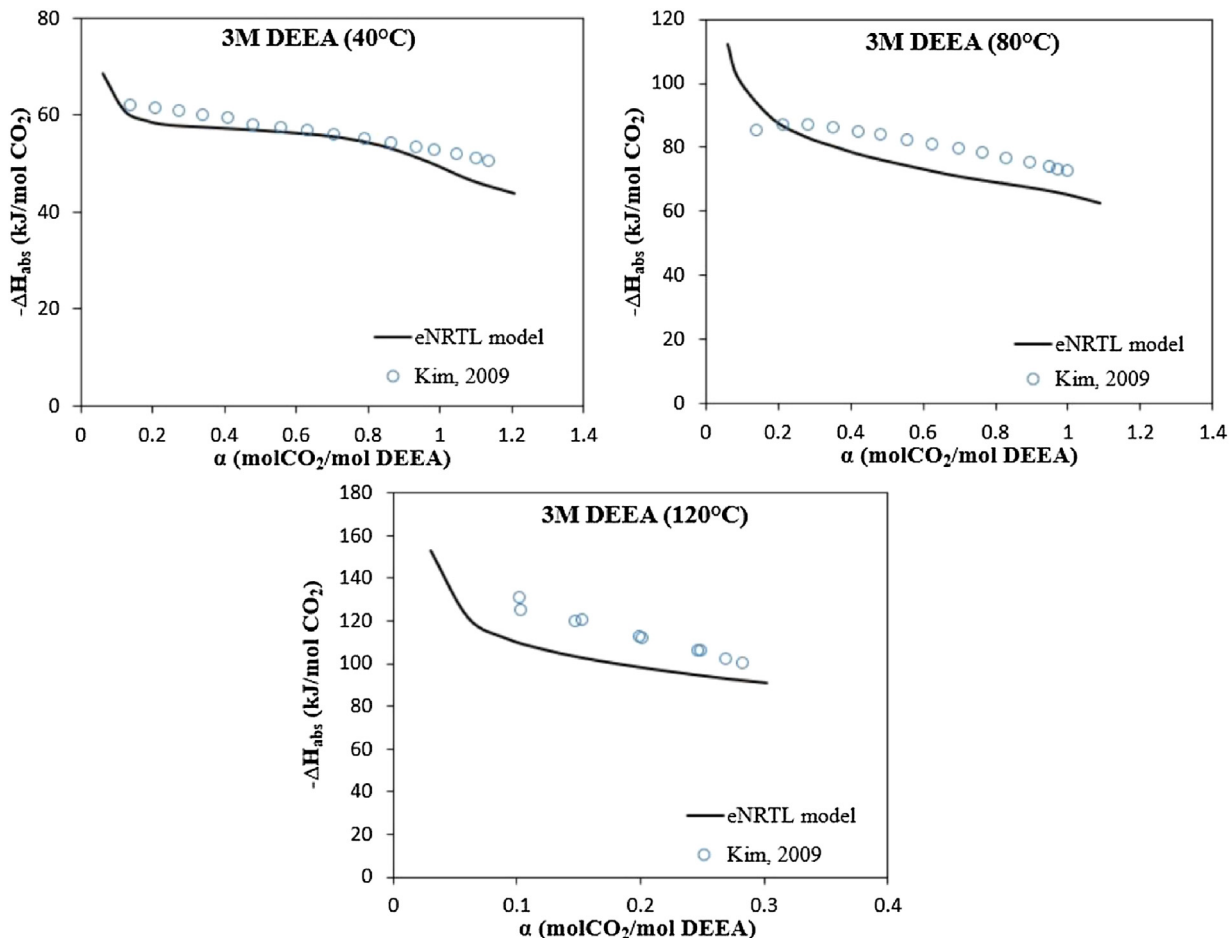


Fig. 7 – Integral heat of CO<sub>2</sub> absorption in 3 M DEEA as function of CO<sub>2</sub> loading at 40, 80 and 120 °C.

The model prediction results of the heat of CO<sub>2</sub> absorption into aqueous solution of 3 M DEEA are compared to experimental results from Kim (2009) at 40, 80 and 120 °C and the results are shown in Fig. 7. The results show a decrease on the heat of CO<sub>2</sub> absorption as the CO<sub>2</sub> loading increases. Moreover, the heat of CO<sub>2</sub> absorption is temperature dependent and it increases with the temperature increase. The integral heats of CO<sub>2</sub> absorption are well estimated by the model with an average deviation of 8.01% from the experimental results. The heats of CO<sub>2</sub> absorption were also calculated for 2.68 M (Fig. SI.2), 4 M (Fig. SI.3) and 5 M DEEA (Fig. SI.4) and the average deviations were estimated to respectively 5.81%, 8.02% and 10.17%.

### 3.3.2. MAPA based system

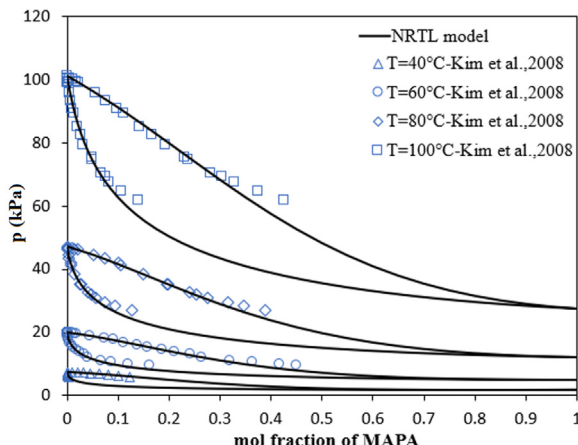
The binary interaction parameters between MAPA and H<sub>2</sub>O were already available in Aspen Plus™ database and are given in Table 5.

A good correlation of MAPA-H<sub>2</sub>O binary vapor-liquid equilibrium can be observed between the NRTL model results and the experimental data from Kim et al. (2008) with an AARD of 2.73% as shown in Fig. 8.

The same assumption as for DEEA system was adopted in the case of MAPA system for the regression of cation (or anion)-molecule pair interaction parameters. The interaction parameters involving species that are present in low concentrations such as CO<sub>2</sub>(aq), OH<sup>-</sup>, H<sub>3</sub>O<sup>+</sup> and MAPAH<sup>+</sup> were not

**Table 5 – Aspen Plus™ database MAPA-H<sub>2</sub>O NRTL parameters.**

| Parameter        | Component m      | Component m'     | Value   |
|------------------|------------------|------------------|---------|
| A <sub>mm'</sub> | MAPA             | H <sub>2</sub> O | -0.2055 |
| A <sub>m'm</sub> | H <sub>2</sub> O | MAPA             | 13.138  |
| B <sub>mm'</sub> | MAPA             | H <sub>2</sub> O | -1635.5 |
| B <sub>m'm</sub> | H <sub>2</sub> O | MAPA             | -2433.2 |
| $\alpha_{mm'}$   | H <sub>2</sub> O | MAPA             | 0.1     |

**Fig. 8 – MAPA-H<sub>2</sub>O vapor-liquid equilibrium as function of MAPA mole fraction at 40, 60, 80 and 100 °C.**

regressed. The non-regressed parameters were set to default values, as given previously. The 20 remaining cation (or anion)-molecule pair interaction parameters were regressed using experimental VLE data from Arshad et al. (2014) and the results are shown in Table 6.

The CO<sub>2</sub> partial pressure and total pressure modeling results for 1 M (8.9 wt%) and 2 M (17.87 wt%) MAPA solutions are presented along with experimental results from Arshad et al. (2014) at 40, 80 and 120 °C and Pinto (2014) (only few data at 2 M MAPA) in Fig. 9.

A good agreement between experimental data and modeling results can be observed for total pressure as function of the CO<sub>2</sub> loading with an AARD of 22.82% and 24.41% respectively for 1 M MAPA and 2 M MAPA. However, higher deviations were observed in the case of CO<sub>2</sub> partial pressure as function of the CO<sub>2</sub> loading with an estimated deviation (AARD) of 39.91% for 1 M MAPA and 38.85% for 2 M MAPA. This deviation might be related to the fact that the CO<sub>2</sub> partial pressures reported in Arshad et al. (2014) are an estimation from the total pressures and only the total pressures have been used in the fitting procedure. Moreover, compared to DEEA-based system the deviation is higher in the case of MAPA-based system. Indeed,

in the case of MAPA system there are more ionic species which means more interactions, but unfortunately less experimental data are available. Moreover, a lack of experimental data at low CO<sub>2</sub> partial pressures is observed for MAPA-based systems in the literature.

The predicted speciation results for MAPA system were compared to experimental data from Perinu et al. (2019) as shown in Fig. 10 (left) for 1 M MAPA and to experimental data from Ciftja et al. (2013) in Fig. 10 (right) for 3.37 M MAPA. Perinu et al. (2019) have identified from the NMR study of MAPA system: primary MAPA carbamates and protonated primary carbamates (MAPACOO<sup>-</sup>(p)/MAPAH<sup>+</sup>COO<sup>-</sup>(p)), secondary MAPA carbamates and protonated secondary carbamates (MAPACOO<sup>-</sup>(s)/MAPAH<sup>+</sup>COO<sup>-</sup>(s)) and dicarbamates (MAPA(COO<sup>-</sup>)<sub>2</sub>). All these species being reported as MAPA-CO<sub>2</sub> since in our study only primary MAPA carbamates were considered. MAPA, MAPAH<sup>+</sup>, H<sup>+</sup>MAPAH<sup>+</sup> species are simply reported as MAPA because the NMR method used in Perinu et al. (2019) does not allow differentiating their corresponding amounts.

The mole fraction of MAPA species is constantly decreasing as function of the loading until around 0.6 mol CO<sub>2</sub>/mol MAPA where it starts to increase. While MAPA-CO<sub>2</sub> species are continuously increasing until a loading of around 0.6 mol CO<sub>2</sub>/mol MAPA and then it starts to decrease. The formation of HCO<sub>3</sub><sup>-</sup> + CO<sub>3</sub><sup>2-</sup> is slow at low CO<sub>2</sub> loading and then it increases sharply when MAPA-CO<sub>2</sub> species start to decrease. A change in the slope of the curves can be observed from a loading of about 0.75 mol CO<sub>2</sub>/mol amine. According to Perinu et al. (2019) this change may be related to the hydrolyses of MAPA carbamate species leading to the formation of protonated MAPA species and HCO<sub>3</sub><sup>-</sup>. Globally, the predicted speciation matches quite well the experimental results until a loading of around 0.6 mol CO<sub>2</sub>/mol MAPA, then a deviation can be observed at higher loadings. In addition to these comparisons, a detailed calculated speciation for 1 M MAPA at 40 °C is shown in Fig. SI.9 in part 3 of Supplementary Information dedicated to the modeled speciation.

Fig. 11 shows a comparison of the model prediction and experimental data of Arshad et al. (2013) for the integral heat of CO<sub>2</sub> absorption into 2 M MAPA at 40, 80 and 120 °C as function of the CO<sub>2</sub> loading. Compared to the experimental data, the model results are well at 40 and 80 °C but higher at 120 °C. The deviation is estimated to 5.28%. The heats of CO<sub>2</sub> absorption were also calculated for 0.9 M (Fig. SI.5 left) and 1 M MAPA (Fig. SI.5 right) at 40 °C, 80 °C and 120 °C and the average deviations were estimated to 15.21% and 10.73% respectively. The findings are similar, the model represents well the experimental data at 40 and 80 °C but higher deviation is observed at 120 °C.

**Table 6 – MAPA-H<sub>2</sub>O-CO<sub>2</sub> system cation (or anion)-molecule pair regressed results.**

| Component m/ca   | Component m/ca   | A <sub>m,ca</sub> /A <sub>ca,m</sub> | B <sub>m,ca</sub> /B <sub>ca,m</sub> |
|--|--|--------------------------------------|--------------------------------------|
| H <sub>2</sub> O<br>(H <sup>+</sup> MAPAH <sup>+</sup> , HCO <sub>3</sub> <sup>-</sup> ) | (H <sup>+</sup> MAPAH <sup>+</sup> , HCO <sub>3</sub> <sup>-</sup> ) | 7.7811                               | 202.97                               |
| H <sub>2</sub> O<br>(H <sup>+</sup> MAPAH <sup>+</sup> , CO <sub>3</sub> <sup>2-</sup> ) | H <sub>2</sub> O   | -4.2478                              | 184.37                               |
| H <sub>2</sub> O<br>(H <sup>+</sup> MAPAH <sup>+</sup> , MAPACOO <sup>-</sup> )          | (H <sup>+</sup> MAPAH <sup>+</sup> , CO <sub>3</sub> <sup>2-</sup> ) | 9.9325                               | 445.02                               |
| H <sub>2</sub> O<br>(H <sup>+</sup> MAPAH <sup>+</sup> , MAPACOO <sup>-</sup> )          | H <sub>2</sub> O   | -4.1949                              | -111.65                              |
| MAPA<br>(H <sup>+</sup> MAPAH <sup>+</sup> , CO <sub>3</sub> <sup>2-</sup> )             | (H <sup>+</sup> MAPAH <sup>+</sup> , MAPACOO <sup>-</sup> )          | 11.379                               | 1498.9                               |
| MAPA<br>(H <sup>+</sup> MAPAH <sup>+</sup> , MAPACOO <sup>-</sup> )                      | H <sub>2</sub> O   | -4.1579                              | -646.71                              |
| MAPA<br>(H <sup>+</sup> MAPAH <sup>+</sup> , MAPACOO <sup>-</sup> )                      | (H <sup>+</sup> MAPAH <sup>+</sup> , CO <sub>3</sub> <sup>2-</sup> ) | 76.123                               | -311.48                              |
| MAPA<br>(H <sup>+</sup> MAPAH <sup>+</sup> , MAPACOO <sup>-</sup> )                      | MAPA   | -9.7445                              | -350.96                              |
| MAPA<br>(H <sup>+</sup> MAPAH <sup>+</sup> , MAPACOO <sup>-</sup> )                      | (H <sup>+</sup> MAPAH <sup>+</sup> , MAPACOO <sup>-</sup> )          | 69.761                               | -235.32                              |
| MAPA<br>(H <sup>+</sup> MAPAH <sup>+</sup> , MAPACOO <sup>-</sup> )                      | MAPA   | 53.478                               | 249.83                               |

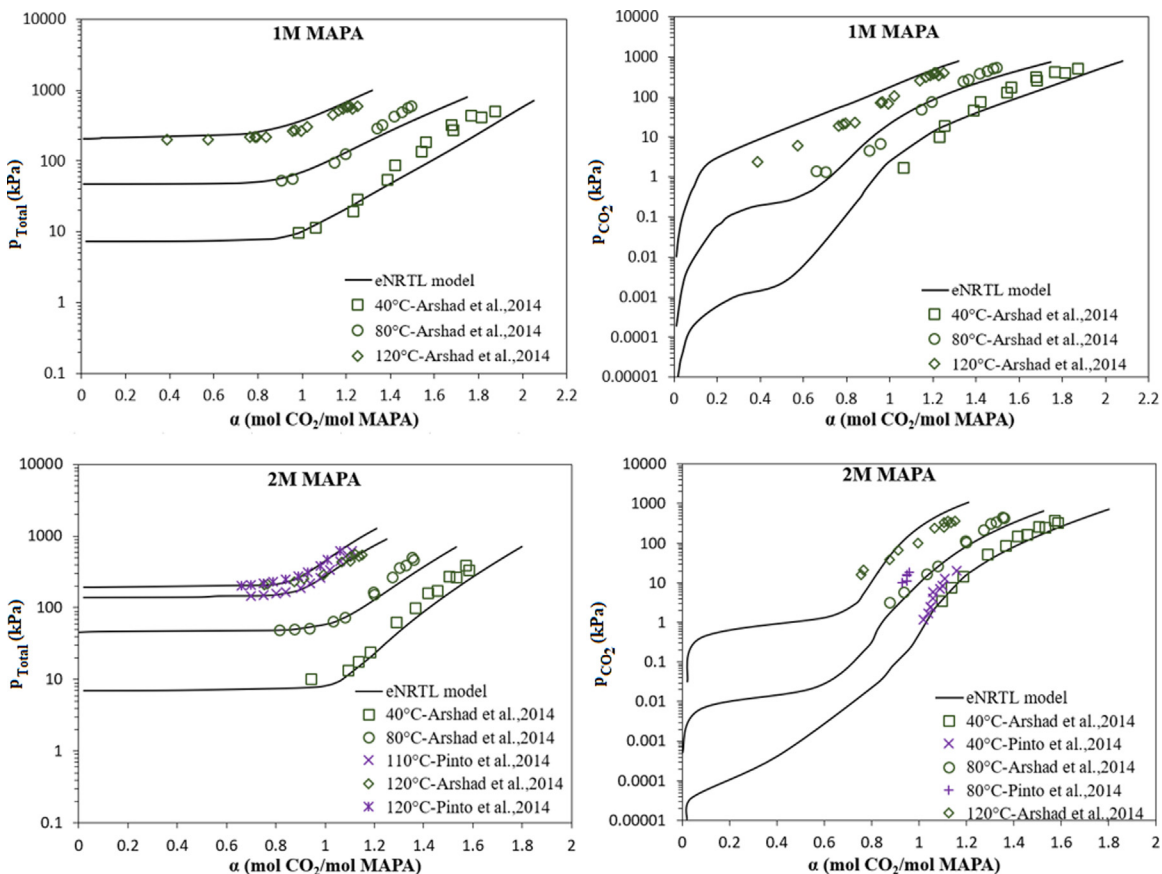


Fig. 9 – Total pressure (left) and  $\text{CO}_2$  partial pressure (right) for 1 M MAPA (top) and 2 M MAPA (bottom) as function of the loading.

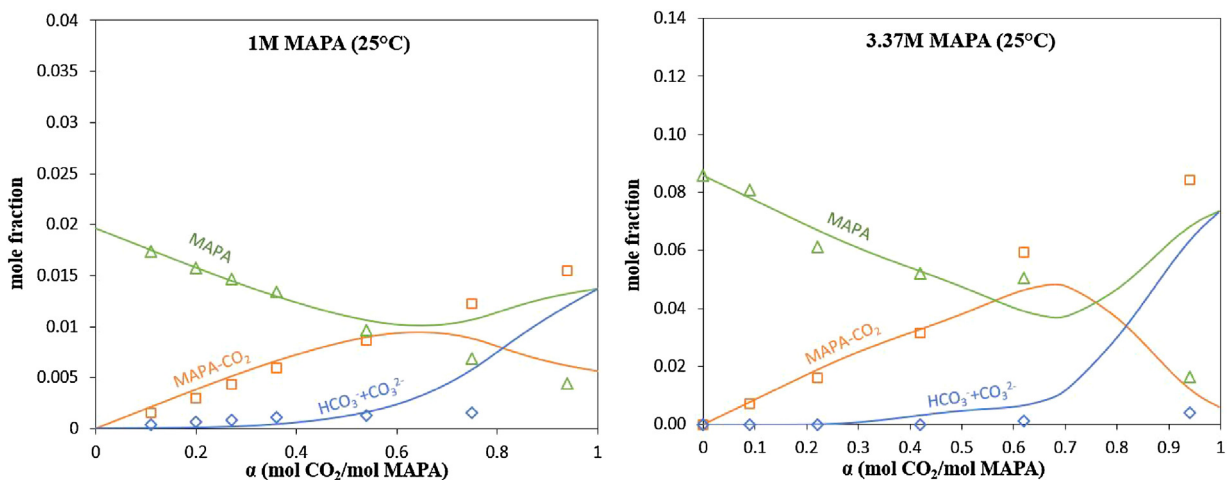


Fig. 10 – Speciation for 1 M MAPA (left) and 3.37 M MAPA (right) at 25 °C model results (solid lines) versus experimental data (open points) from Perinu et al. (2019).

### 3.3.3. DEEA-MAPA based system

In order to accurately model DEEA-MAPA-H<sub>2</sub>O-CO<sub>2</sub> system, additional interaction parameters were estimated. These parameters are the binary and cation (or anion)-molecule pair parameters related to the interaction between the two sub-systems. The binary interaction parameters between MAPA and DEEA were regressed using experimental VLE data of DEEA-MAPA system at different temperatures (80, 100 and 120 °C) from Hartono et al. (2013). The binary interaction parameters together with the non-randomness parameter are shown in Table 7. Due to limitation of experimental data, the regression was carried out to determine the binary parameters while

the non-randomness parameter was fixed to a value of 0.3 as indicated in Renon and Prausnitz (1968).

Fig. 12 shows a comparison between calculated results and experimental data of binary VLE. The model gives a good representation of the experimental data with an average deviation of 3.93% for the binary VLE data compared to experimental results from Hartono et al. (2013).

### 3.3.4. DEEA-MAPA-H<sub>2</sub>O-CO<sub>2</sub> system

For the regression of cation (or anion)-molecule pair parameters of DEEA-MAPA-H<sub>2</sub>O-CO<sub>2</sub> system, the calculated parameters of the two sub-systems DEEA-H<sub>2</sub>O-CO<sub>2</sub> and MAPA-H<sub>2</sub>O-CO<sub>2</sub> separately were used as a basis. Then, addi-

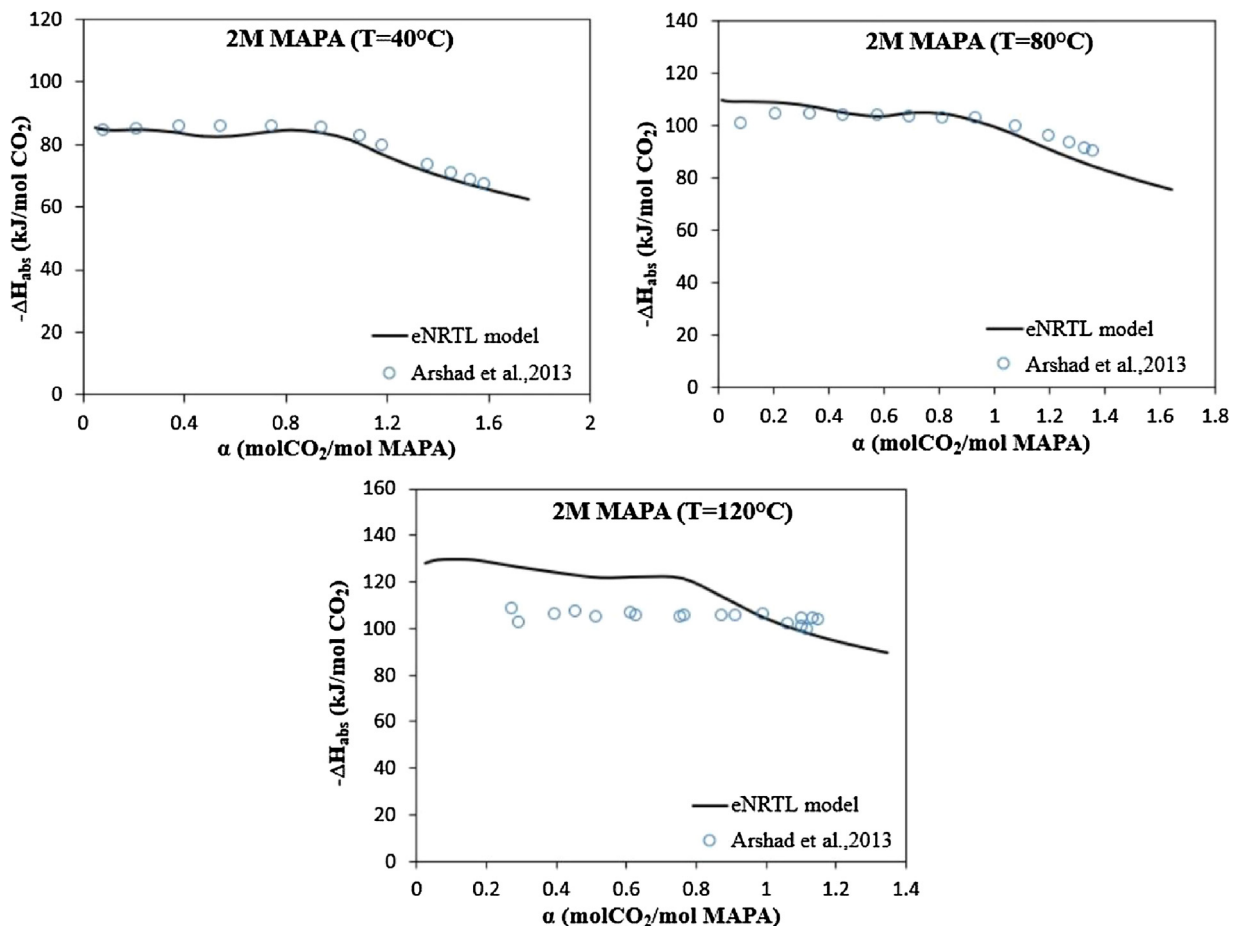


Fig. 11 – Integral heat of CO<sub>2</sub> absorption for 17.9 wt% MAPA at 40, 80 and 120 °C as function of the CO<sub>2</sub> loading.

Table 7 – Regression results of DEEA-MAPA NRTL binary parameters.

| Parameter        | Component m | Component m' | Value   |
|------------------|-------------|--------------|---------|
| A <sub>mm'</sub> | MAPA        | DEEA         | -0.6204 |
| A <sub>m'm</sub> | DEEA        | MAPA         | 0.5812  |
| B <sub>mm'</sub> | MAPA        | DEEA         | -257.44 |
| B <sub>m'm</sub> | DEEA        | MAPA         | 188.74  |
| $\alpha_{mm'}$   | DEEA        | MAPA         | 0.3     |

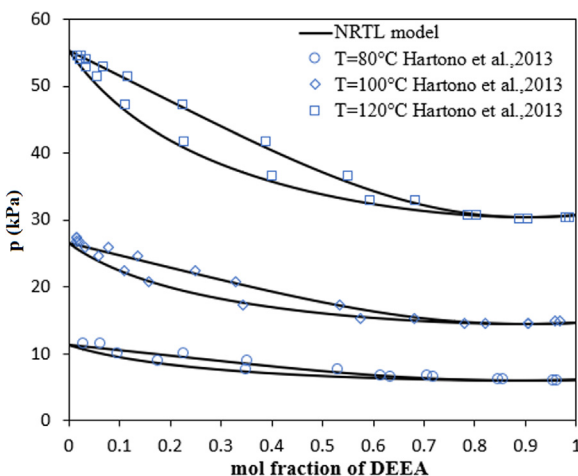


Fig. 12 – DEEA-MAPA vapor-liquid equilibrium as function of DEEA mole fraction at 80, 100 and 120 °C.

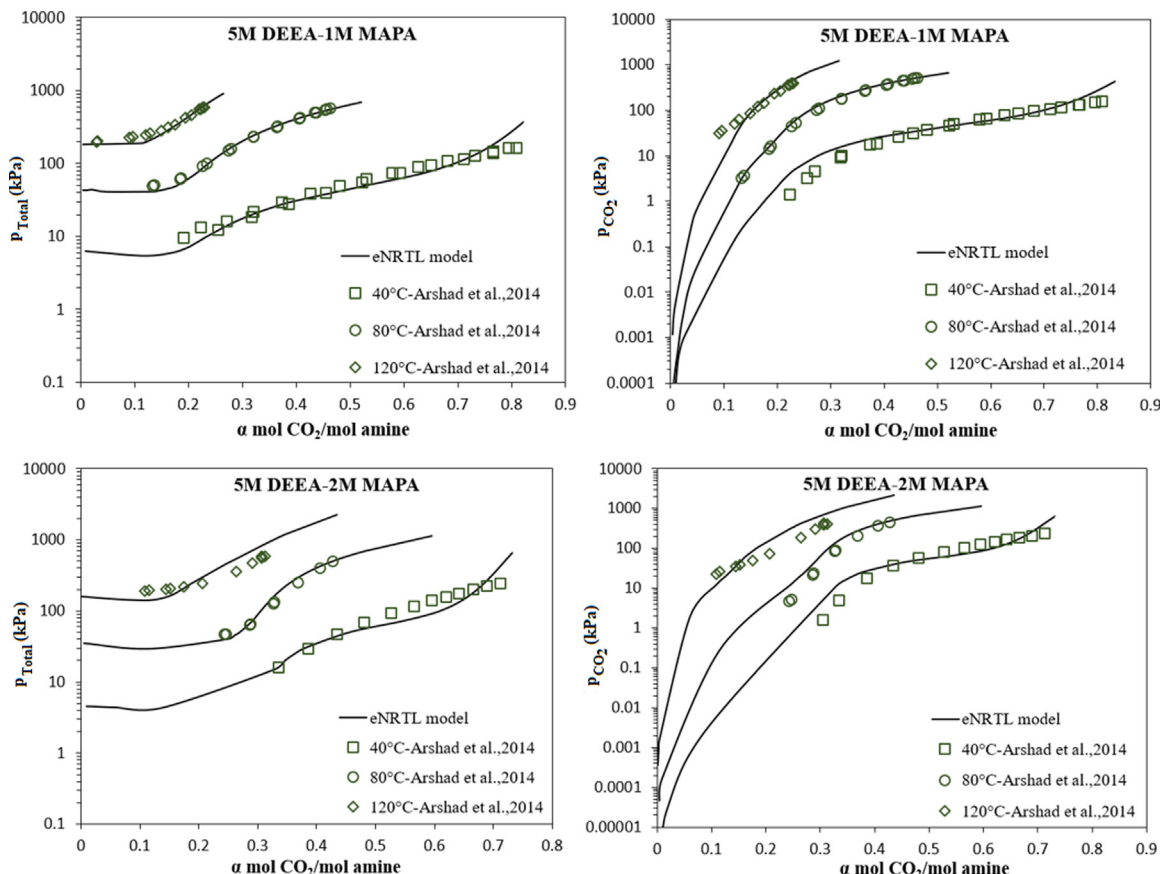
tional parameters related to the interactions between the two systems were calculated. The same hypothesis was considered in order to regress only the relevant combinations. The

principle is to not regress the interaction parameters involving a species at very low concentrations in the system such as CO<sub>2</sub>(aq), OH<sup>-</sup>, H<sub>3</sub>O<sup>+</sup>, CO<sub>3</sub><sup>2-</sup> and MAPAH<sup>+</sup>. The non-regressed parameters were set to default values, as noted before. Therefore, 24 cation (or anion)-molecule pair interaction parameters were regressed using experimental VLE data from Arshad et al. (2014) and the results are shown in Table 8.

The results of the total pressure and partial pressure as function of the CO<sub>2</sub> loading are presented in Fig. 13 for two mixtures namely 5 M DEEA-1 M MAPA and 5 M DEEA-2 M MAPA at 40, 80 and 120 °C. Both these mixtures can lead to liquid-liquid phase separation upon CO<sub>2</sub> absorption. Not all DEEA-MAPA loaded mixtures can lead to a liquid-liquid phase separation, for example no phase separation was observed in the case of 4 M DEEA-1 M MAPA and 3 M DEEA-2 M MAPA mixtures. All these different behaviors make aqueous DEEA-MAPA mixtures very challenging and interesting to be studied. As observed in Fig. 13, the developed model represents fairly well the experimental data (Arshad et al., 2014) of the total pressure with an AARD of 10.93% for 5 M DEEA-1 M MAPA and AARD of 18.92% for CO<sub>2</sub> partial pressure. In the case of 5 M DEEA-2 M MAPA, the AARD was estimated to 21.55% for total pressure and 37.77% for CO<sub>2</sub> partial pressure. It can be seen that the deviation is mainly observed at low pressure and at 120 °C. It is important to highlight that the deviation is always higher for the CO<sub>2</sub> partial pressure, the experimental data are an estimation from the total pressure and only total pressure results have been used in the fitting procedure. It can be noted that the eNRTL parameters used in the model for both DEEA-based system, MAPA-based system and DEEA-MAPA global system are summarized in section 4 of Supplementary Information.

**Table 8 – DEEA-MAPA-H<sub>2</sub>O-CO<sub>2</sub> system additional cation (or anion)-molecule pairs regressed results.**

| Component m/ca   | Component m/ca   | A <sub>m,ca/A<sub>ca,m</sub></sub> | B <sub>m,ca/B<sub>ca,m</sub></sub> |
|--|--|------------------------------------|------------------------------------|
| H <sub>2</sub> O   | (DEEAH <sup>+</sup> , MAPACOO <sup>-</sup> )                         | 7.2203                             | -414.43                            |
| (DEEAH <sup>+</sup> , MAPACOO <sup>-</sup> )                         | H <sub>2</sub> O   | -3.6905                            | -34.221                            |
| MAPA   | (DEEAH <sup>+</sup> , HCO <sub>3</sub> <sup>-</sup> )                | -4.0736                            | 3.719                              |
| (DEEAH <sup>+</sup> , HCO <sub>3</sub> <sup>-</sup> )                | MAPA   | 52.303                             | 5.4112                             |
| MAPA   | (DEEAH <sup>+</sup> , MAPACOO <sup>-</sup> )                         | 39.759                             | 3.2380                             |
| (DEEAH <sup>+</sup> , MAPACOO <sup>-</sup> )                         | MAPA   | -7.1380                            | -0.3190                            |
| DEEA   | (DEEAH <sup>+</sup> , MAPACOO <sup>-</sup> )                         | 15.319                             | -4.3788                            |
| (DEEAH <sup>+</sup> , MAPACOO <sup>-</sup> )                         | DEEA   | -2.6551                            | 42.111                             |
| DEEA   | (H <sup>+</sup> MAPAH <sup>+</sup> , HCO <sub>3</sub> <sup>-</sup> ) | 4.4745                             | -44.709                            |
| (H <sup>+</sup> MAPAH <sup>+</sup> , HCO <sub>3</sub> <sup>-</sup> ) | DEEA   | 11.4530                            | 18.209                             |
| DEEA   | (H <sup>+</sup> MAPAH <sup>+</sup> , MAPACOO <sup>-</sup> )          | -0.9881                            | 484.56                             |

**Fig. 13 – Total pressure (left) and CO<sub>2</sub> partial pressure (right) for 5 M DEEA-1 M MAPA (top) and 5 M DEEA-2 M MAPA (bottom) mixtures as function of the loading at 40, 80 and 120 °C.**

A comparison between the speciation predicted results and experimental data from Perinu et al. (2019) is shown in Fig. 14 for 3 M DEEA-1 M MAPA mixture at 25 °C. Here also, primary MAPA carbamates and protonated primary carbamates (MAPACOO<sup>-</sup>(p)/MAPAH<sup>+</sup>COO<sup>-</sup>(p)), secondary MAPA carbamates and protonated secondary carbamates (MAPACOO<sup>-</sup>(s)/MAPAH<sup>+</sup>COO<sup>-</sup>(s)) and dicarbamates (MAPA(COO<sup>-</sup>)<sub>2</sub>) species are reported as MAPA-CO<sub>2</sub> since in the present study only primary MAPA carbamates were considered. MAPA, MAPAH<sup>+</sup>, H<sup>+</sup>MAPAH<sup>+</sup> species are reported as MAPA. It can be observed that, DEEA reacts weakly with CO<sub>2</sub> while MAPA reacts directly with CO<sub>2</sub> to form mainly MAPA-CO<sub>2</sub> species. After that MAPA is almost fully consumed, more DEEA reacts with CO<sub>2</sub> to form DEEAH<sup>+</sup> and HCO<sub>3</sub><sup>-</sup> while MAPA-CO<sub>2</sub> reach a maximum and stabilize. Like MAPA-CO<sub>2</sub> based system, a similar change in the slope of the curves can be observed from a loading of about 0.75 mol CO<sub>2</sub>/mol amine corresponding to the hydrolyses of MAPA

carbamate species. Overall, the model speciation results are in good agreement with the experimental data especially until 0.5 mol CO<sub>2</sub>/mol amine. Over this value the difference is slightly higher for MAPA, HCO<sub>3</sub><sup>-</sup>+CO<sub>3</sub><sup>2-</sup> and MAPA-CO<sub>2</sub> species, whereas an important disparity in the experimental results can be observed for DEEA + DEEAH<sup>+</sup> species.

The detailed model calculated speciation of 5 M DEEA-2 M MAPA mixture at 40 °C is presented in Fig. S1.9 in Supplementary Information.

The calculated integral heats of CO<sub>2</sub> absorption are presented for two amine mixtures; 3.12 M DEEA-0.34 M MAPA and 5 M DEEA-2 M MAPA at 40 and 120 °C in Fig. 15. It can be seen that, the experimental data at 3.12 M (37 wt%) DEEA-0.34 M (3 wt%) MAPA from Kim (2009) and the model results are in good agreement with a relative deviation of 10.88%. The calculated integral heats of CO<sub>2</sub> absorption were also compared to experimental results from Arshad et al. (2013) for 5 M DEEA-2 M MAPA mixture. The results seem satisfactory with

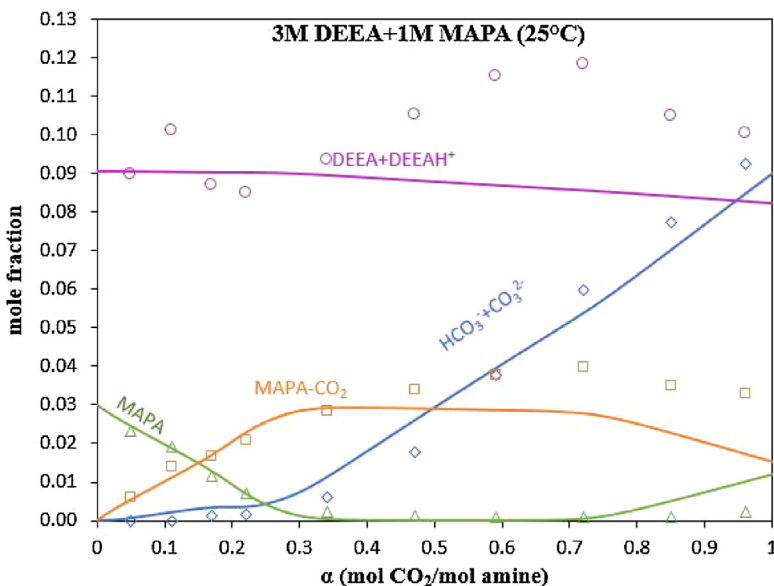


Fig. 14 – 3 M DEEA-1 M MAPA speciation; model results (solid lines) versus experimental data (open points) from Perinu et al. (2019) at 25 °C.

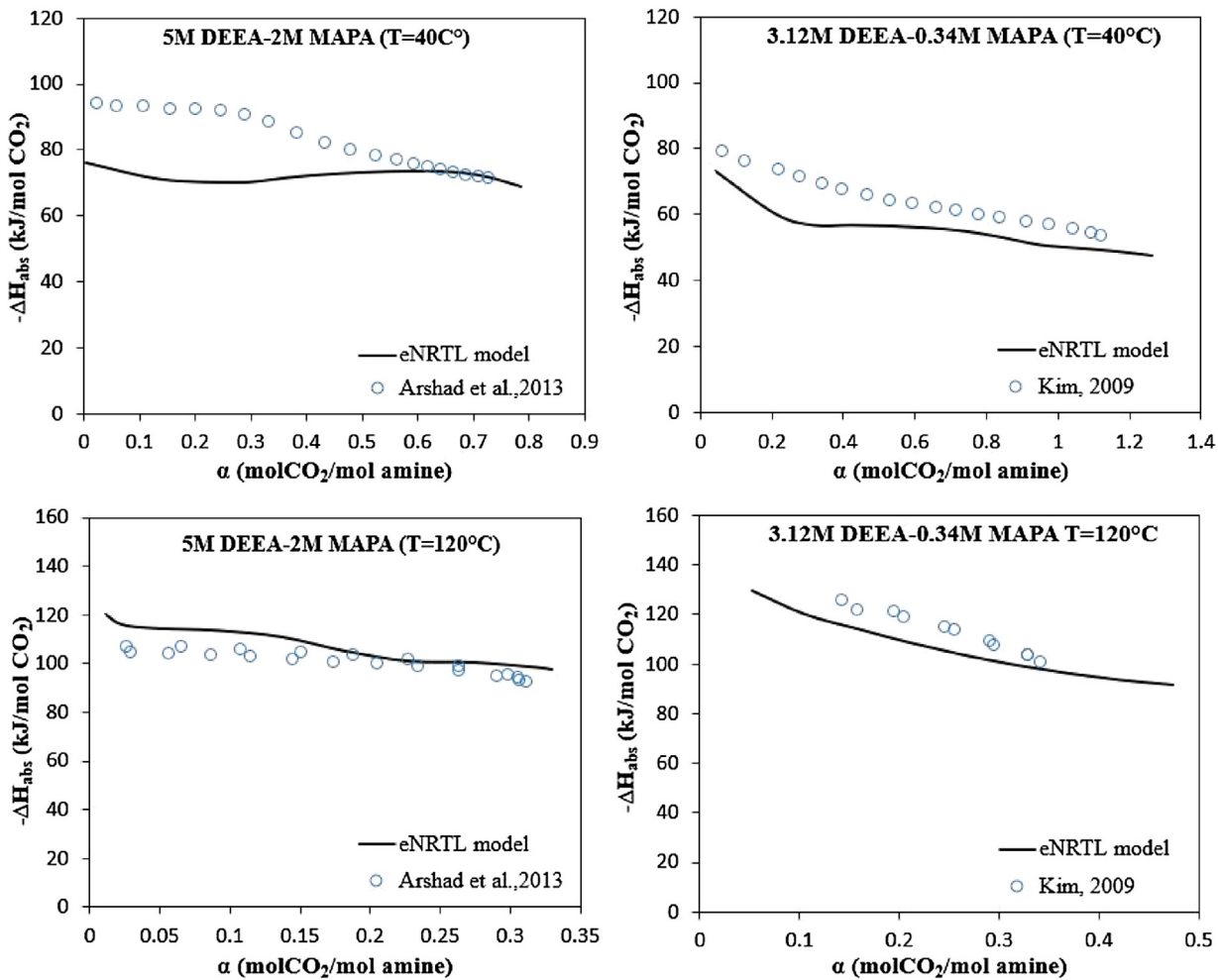


Fig. 15 – Integral heat of CO<sub>2</sub> absorption in 3.12 M DEEA-0.34 M MAPA (left) and 5 M DEEA-2 M MAPA (right) as function of CO<sub>2</sub> loading at 40 and 120 °C.

a small deviation at 40 °C below a loading of 0.5 molCO<sub>2</sub>/mol amine, the AARD was 7.23%. The heats of CO<sub>2</sub> absorption were also calculated for other amine mixtures as shown in Supplementary Information (Fig. SI.6). The AARD was 22.39% for 2.69

M DEEA-0.89 M MAPA and of 5.8% for 5 M DEEA-1 M MAPA mixtures.

As mentioned before, 5 M DEEA-2 M MAPA is a mixture that splits into two liquid phases when loaded with CO<sub>2</sub>. Only few

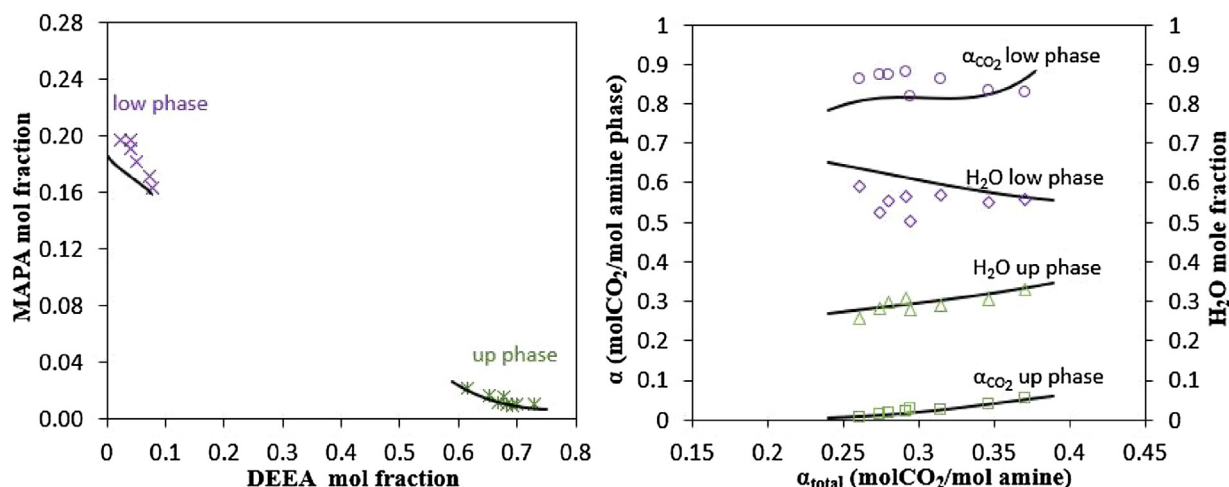


Fig. 16 – Liquid-liquid equilibrium results: amine distribution (left),  $\text{CO}_2$  loading and  $\text{H}_2\text{O}$  distribution (right) at 40 °C, model results (solid lines) versus experimental data (open points) from Pinto et al. (2014b).

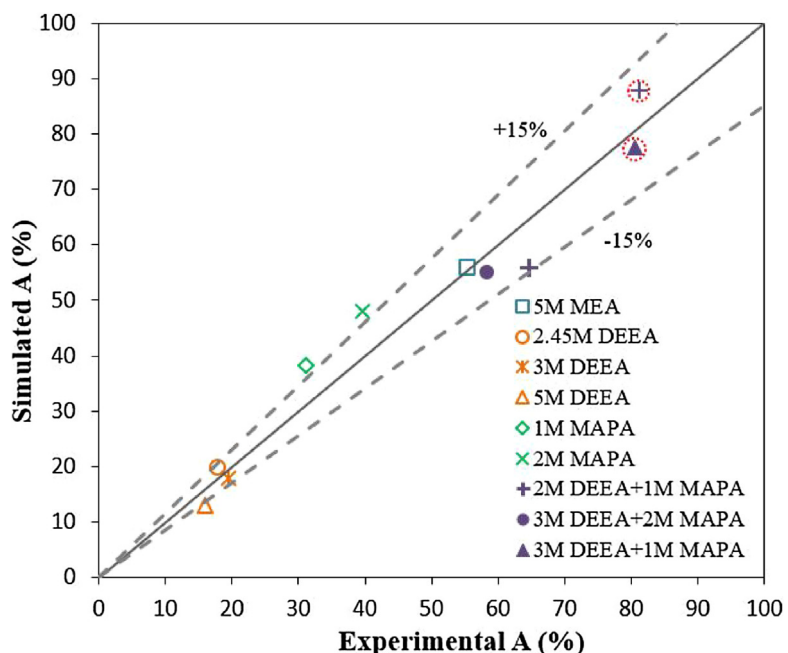


Fig. 17 – Parity plot of simulated versus experimental UMONS micro-pilot unit results of  $\text{CO}_2$  absorption rate with  $y_{\text{CO}_2}$  of 20 mol.% (two encircled symbols with  $y_{\text{CO}_2}$  of 10 mol.%).

liquid-liquid equilibrium experimental data were available in Pinto et al. (2014b) for this mixture. The developed model was able to predict the demixing phenomenon. First, the solution is loaded with  $\text{CO}_2$  in a flash unit, then the resulting loaded solution is sent to the decanter where it is separated into two liquid phases. However, it is important to have a good species distribution in the two phases for the process simulation as only the  $\text{CO}_2$  rich phase is sent to the regeneration column.

A correlation between the loading and the species mole fraction in each phase was introduced for fitting correctly with the experimental data. Hence, the liquid-liquid phase separation was calculated using a decanter unit where the phase split was calculated by equating the fugacities of the components in the two liquid phases and the liquid-liquid coefficients were calculated from the liquid-liquid distribution coefficients (KLL) correlations. Details about these correlations are given in part 5 of Supplementary Information. The modeled and experimental species distribution in the lower and upper phase are shown in Fig. 16.

Fig. 16 (left) shows DEEA and MAPA species distribution where the lower (heavy) phase is mainly constituted of MAPA while DEEA is mainly concentrated in the upper (light) phase. The  $\text{CO}_2$  content of each phase is also shown in Fig. 16 (right). The  $\text{CO}_2$  loading in each phase is presented as function of the total loading. Clearly, the  $\text{CO}_2$  is concentrated in the lower phase with around 0.9 molCO<sub>2</sub>/mol amine while the upper phase is almost lean on  $\text{CO}_2$ . Regarding the water distribution in the two phases, it seems that the upper phase is hydrophobic with less water content than the lower phase. The modeled results look satisfactory for the phase separation.

#### 4. Simulation and model validation at pilot scale

The purpose of this study was to develop a thermodynamic modeling that can be used for absorption-regeneration process modeling (see part 6.1 of Supplementary Information). Therefore, a comparison between experimental results from

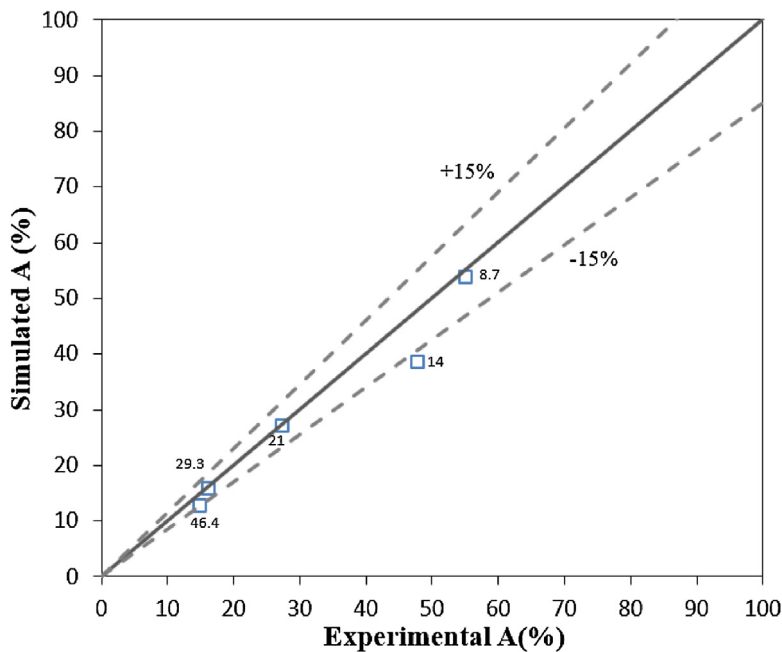


**Fig. 18 – Parity plot of simulated versus experimental (NTNU/SINTEF) pilot unit results of CO<sub>2</sub> absorption rate (the values on the graph represent the CO<sub>2</sub> mol compositions).**

micro-pilot unit and simulation results using the developed model in Aspen Plus<sup>TM</sup> was performed.

The validation of the developed model was realized using both experimental results from the UMONS micro-pilot unit and then from the NTNU/SINTEF pilot campaign. The absorption-regeneration UMONS micro-pilot unit was used in the work of Dubois (2013) and Laribi et al. (2019). The installation is mainly constituted of two stainless steel columns (absorber and stripper) with an inside diameter of 56 mm and easily adjustable packing height ( $H_p$ ) (0.5 m or 1 m), packed with glass Raschig rings (6 × 6 mm) (see part 6.2 of Supplementary Information for more details). Two CO<sub>2</sub> gas compositions have been tested, namely: 20 mol% and 10 mol%. Regarding the amine solutions, several amine concentrations and mixtures have been tested, namely: 5 M MEA, DEEA-based concentrations (2.45 M DEEA, 3 M DEEA, 5 M DEEA), MAPA-based concentrations (1 M MAPA, 2 M MAPA), and DEEA-MAPA mixtures (2 M DEEA-1 M MAPA, 3 M DEEA-2 M MAPA and 3 M DEEA-1 M MAPA).

A successful comparison between the simulated and experimental results based on absorption rate (A%) is shown in Fig. 17. From the parity plot it can be seen that almost all the results present a deviation lower than 20%.

In order to complete the previous validation with another amine mixture, experimental data from NTNU/SINTEF micro-pilot campaign (Pinto et al., 2014a) with 5 M DEEA-2 M MAPA demixing mixture at different CO<sub>2</sub> contents were used. The unit is mainly composed of two columns, absorption column with 4.23 m packing height and 0.15 m diameter and the stripper with 3.57 m packing height and 0.1 m diameter (more details on the pilot unit can be found in part 6.3 of Supplementary Information).

Fig. 18 shows a parity plot of CO<sub>2</sub> absorption rate simulated results versus experimental data from the literature at five CO<sub>2</sub> inlet compositions namely; 8.7, 14.0, 21.2, 29.3 and 46.4 vol %. It can be seen that the comparison between experimental data and simulated results shows quite acceptable deviations (lower than 20%) for the absorption rate.

## 5. Conclusion and perspectives

To accurately simulate the CO<sub>2</sub> absorption-regeneration process, a rigorous thermodynamic modeling of the system is required. In this work the electrolyte NRTL model has been developed by several data regressions using Aspen Plus<sup>TM</sup>(V10) tool to describe the thermodynamics of the two subsystems DEEA-H<sub>2</sub>O-CO<sub>2</sub> and MAPA-H<sub>2</sub>O-CO<sub>2</sub> and the global DEEA-MAPA-H<sub>2</sub>O-CO<sub>2</sub> system.

Different types of thermodynamic data (pure amine vapor pressures, excess enthalpies, binary and ternary vapor-liquid equilibria) were used to provide a robust model. As a result, the developed model was able to represent the two subsystems separately and the global DEEA-MAPA-H<sub>2</sub>O-CO<sub>2</sub> system through experimental data of vapor-liquid, liquid-liquid, speciation and heat of CO<sub>2</sub> absorption with good accuracy. The model results of the heat of CO<sub>2</sub> absorption are predictive as the cation (or anion)-molecule pair parameters of the electrolyte NRTL model were regressed using solely the VLE data.

The developed model was successfully validated through two steps. The first one by using experimental results from UMONS micro-pilot unit at different amine and CO<sub>2</sub> compositions. The second step, by simulating experimental NTNU/SINTEF pilot campaign results using 5 M DEEA-2 M MAPA at different CO<sub>2</sub> contents. Globally, the results were satisfactory with a maximum observed deviation of about 20%. The developed model could be used to carry out an evaluation and optimization of CO<sub>2</sub> absorption-regeneration process using DEEA-MAPA mixtures at large scale.

## Conflict of interest

No conflict of interest exists.

## Funding

No funding was received for this work.

## Intellectual property

We confirm that we have given due consideration to the protection of intellectual property associated with this work and that there are no impediments to publication, including the timing of publication, with respect to intellectual property. In so doing we confirm that we have followed the regulations of our institutions concerning intellectual property.

## Research ethics

We further confirm that any aspect of the work covered in this manuscript that has involved human patients has been conducted with the ethical approval of all relevant bod-

ies and that such approvals are acknowledged within the manuscript.

## Acknowledgments

The authors would like to acknowledge the European Cement Research Academy (ECRA) and Heidelberg Cement Company for their technical and financial support.

## Appendix A. Summary on the experimental data used for the regression of the different model parameters and for the validation of the developed model

See [Tables A1–A3](#).

**Table A1 – Experimental data used for the regression and the validation of the developed model for DEEA based system.**

| Data type                        | T (°C)              | Amine composition (M)       | CO <sub>2</sub> loading | References (s)   | AARD (%)                      |
|----------------------------------|---------------------|-----------------------------|-------------------------|--|-------------------------------|
| Vapor pressure                   | 64–160              | Pure DEEA                   | –                       | (Hartono et al., 2013) <sup>R,V</sup>  | 1.5                           |
| Excess enthalpy                  | 25                  | DEEA-H <sub>2</sub> O       | –                       | (Mathonat et al., 1997) <sup>R,V</sup>   | 4.6                           |
| Binary VLE                       | 50,60,80 and 95     | DEEA-H <sub>2</sub> O       | –                       | (Hartono et al., 2013) <sup>R,V</sup>  | 2.33                          |
| Henry constant                   | 45 and 65           | DEEA-H <sub>2</sub> O       | –                       | (Monteiro et al., 2015a) <sup>R</sup><br>(Luo et al., 2016) <sup>V</sup>   | 12.66<br>14.62                |
| CO <sub>2</sub> Partial pressure | 40,60, 80 and 120   | 2 M<br>5 M                  | 0.045–1                 | (Monteiro et al., 2013) <sup>V</sup><br>(Arshad et al., 2014) <sup>V</sup><br>(Monteiro et al., 2013) <sup>V</sup>           | 9<br>19.63<br>14.52           |
| Total pressure                   | 40, 80, 100 and 120 | 2 M<br>5 M                  | 0.045–1                 | (Monteiro et al., 2013) <sup>V</sup><br>(Arshad et al., 2014) <sup>R,V</sup><br>(Monteiro et al., 2013) <sup>V</sup>         | 5.83<br>8.62<br>6.91          |
| Heat of reaction                 | 40,80 and 120       | 2.68 M<br>3 M<br>4 M<br>5 M | 0.09–1                  | (Kim, 2009) <sup>V</sup><br>(Kim, 2009) <sup>V</sup><br>(Xu et al., 2014) <sup>V</sup><br>(Arshad et al., 2013) <sup>V</sup> | 5.81<br>8.01<br>8.02<br>10.17 |
| Speciation                       | 25                  | 2.68 M<br>3 M               | 0–1                     | (Giftja et al., 2013) <sup>V</sup><br>(Perinu et al., 2019) <sup>V</sup>   | –<br>–                        |

**Table A2 – Experimental data used for the regression and the validation of the developed model for MAPA based system.**

| Data type                        | T (°C)            | Amine composition (M)        | CO <sub>2</sub> loading | References (s)   | AARD (%)               |
|----------------------------------|-------------------|------------------------------|-------------------------|--|------------------------|
| Vapor pressure                   | 54–140            | Pure MAPA                    | –                       | (Hartono et al., 2013) <sup>R,V</sup>  | 1                      |
| Excess enthalpy                  | –                 | –                            | –                       | (Kim et al., 2008) <sup>R,V</sup>  | –                      |
| Binary VLE                       | 40,60,80 and 100  | MAPA-H <sub>2</sub> O        | –                       | (Kim et al., 2008) <sup>V</sup>  | 2.73                   |
| Henry constant                   | 45 and 65         | MAPA-H <sub>2</sub> O<br>1 M | –                       | (Monteiro et al., 2014) <sup>V</sup><br>(Arshad et al., 2014) <sup>V</sup>                                 | 5.12<br>39.91          |
| CO <sub>2</sub> partial pressure | 40,80 and 120     | 2 M                          | 0.4–1.8                 | (Arshad et al., 2014) <sup>V</sup><br>(Pinto, 2014) <sup>V</sup>   | 38.85<br>–             |
| Total pressure                   | 40,80,110 and 120 | 1 M<br>2 M                   | 0.4–1.8                 | (Arshad et al., 2014) <sup>R,V</sup><br>(Arshad et al., 2014) <sup>R,V</sup><br>(Pinto, 2014) <sup>V</sup> | 22.82<br>24.41<br>–    |
| Heat of reaction                 | 40,80 and 120     | 0.9 M<br>1 M<br>2 M          | 0.04–2                  | (Kim, 2009) <sup>V</sup><br>(Arshad et al., 2013) <sup>V</sup><br>(Arshad et al., 2013) <sup>V</sup>       | 15.21<br>10.73<br>5.28 |
| Speciation                       | 25                | 1 M<br>3.37 M                | 0–1.6<br>0–1            | (Perinu et al., 2019) <sup>V</sup><br>(Giftja et al., 2013) <sup>V</sup>                                   | –<br>–                 |

**Table A3 – Additional experimental data used for the regression and the validation of the developed model for DEEA-MAPA-H<sub>2</sub>O-CO<sub>2</sub> global system.**

| Data type                        | T (°C)          | Amine composition (M)                                       | CO <sub>2</sub> loading | References (s)   | AARD (%)             |
|----------------------------------|-----------------|---|-------------------------|--|----------------------|
| Binary VLE                       | 80, 100 and 120 | DEEA-MAPA   | –                       | (Hartono et al., 2013) <sup>V,R</sup>  | 3.93                 |
| CO <sub>2</sub> partial pressure | 40,80 and 120   | 5M DEEA-1M MAPA<br>5M DEEA-2M MAPA                          | 0.1–0.8                 | (Arshad et al., 2014) <sup>V</sup>   | 18.92<br>37.77       |
| Total pressure                   | 40,80 and 120   | 5M DEEA-1M MAPA<br>5M DEEA-2M MAPA                          | 0.1–0.8                 | (Arshad et al., 2014) <sup>R,V</sup><br>(Arshad et al., 2014) <sup>R,V</sup>                         | 18.92<br>21.55       |
| Heat of reaction                 | 40,80 and 120   | 3.12M DEEA-0.34M MAPA<br>5M DEEA-2M MAPA<br>5M DEEA-1M MAPA | 0.02–0.9                | (Kim, 2009) <sup>V</sup><br>(Arshad et al., 2013) <sup>V</sup><br>(Arshad et al., 2013) <sup>V</sup> | 10.88<br>7.23<br>5.8 |

– Table A3 (Continued)

| Data type                            | T (°C) | Amine composition (M) | CO <sub>2</sub> loading | References (s)                     | AARD (%) |
|--------------------------------------|--------|-----------------------|-------------------------|------------------------------------|----------|
| Liquid-liquid-equilibrium Speciation | 40     | 2.69M DEEA-0.89M MAPA | 0.26–0.37<br>0–1        | (Kim, 2009) <sup>V</sup>           | 22.39    |
|                                      |        | 5M DEEA-2M MAPA       |                         | (Pinto, 2014) <sup>R,V</sup>       | –        |
|                                      |        | 3M DEEA-1MMAPA        |                         | (Perinu et al., 2019) <sup>V</sup> | –        |

Note: <sup>R</sup> for regression and <sup>V</sup> for validation.

## Appendix B. Supplementary Information

Supplementary material related to this article can be found, in the online version, at doi:<https://doi.org/10.1016/j.cherd.2020.02.029>.

## References

- Arshad, M.W., Fosbøl, P.L., Von Solms, N., Svendsen, H.F., Thomsen, K., 2013. Heat of absorption of CO<sub>2</sub> in phase change solvents: 2-(diethylamino)ethanol and 3-(methylamino)propylamine. *J. Chem. Eng. Data* 58, 1974–1988 <https://doi.org/10.1021/je400289v>.
- Arshad, M.W., Svendsen, H.F., Fosbøl, P.L., Von Solms, N., Thomsen, K., 2014. Equilibrium total pressure and CO<sub>2</sub> solubility in binary and ternary aqueous solutions of 2-(diethylamino)ethanol (DEEA) and 3-(methylamino)propylamine (MAPA). *J. Chem. Eng. Data* 59, 764–774 <https://doi.org/10.1021/je400886w>.
- Arshad, M.W., von Solms, N., Thomsen, K., 2016. Thermodynamic modeling of liquid-liquid phase change solvents for CO<sub>2</sub> capture. *Int. J. Greenh. Gas Control* 53, 401–424 <https://doi.org/10.1016/j.ijggc.2016.08.014>.
- Austgen, D.M., Rochelle, G.T., Chen, C.C., Peng, X., 1989. Model of vapor-liquid equilibria for aqueous acid gas–alkanolamine systems using the electrolyte-NRTL equation. *Ind. Eng. Chem. Res.* 28, 1060–1073 <https://doi.org/10.1021/ie00091a028>.
- Bernhardsen, I.M., Krokvik, I.R.T., Perinu, C., Pinto, D.D.D., Jens, K.J., Knuutila, H.K., 2018. Influence of pKa on solvent performance of MAPA promoted tertiary amines. *Int. J. Greenh. Gas Control* 68, 68–76 <https://doi.org/10.1016/j.ijggc.2017.11.005>.
- Brüder, P., Owrang, F., Svendsen, H.F., 2012. Pilot study-CO<sub>2</sub> capture into aqueous solutions of 3-methylaminopropylamine (MAPA) activated dimethyl-monoethanolamine (DMMEA). *Int. J. Greenh. Gas Control* 11, 98–109 <https://doi.org/10.1016/j.ijggc.2012.07.004>.
- Chen, C.C., Evans, L.B., 1986. A local composition model for the excess Gibbs energy of aqueous electrolyte systems. *AIChE J.* 32, 444–454 <https://doi.org/10.1002/aic.690320311>.
- Chen, X., Rochelle, G.T., 2013. Thermodynamics of CO<sub>2</sub>/2-methylpiperazine/Water. *Ind. Eng. Chem. Res.* 52, 4229–4238.
- Chen, C., Britt, H.l., Boston, J.F., Evans, L.B., 1982. Local composition model for the excess Gibbs energy of aqueous electrolyte systems. *AIChE J.* 28, 588–596.
- Ciftja, A.F., Hartono, A., Svendsen, H.F., 2013. Experimental study on phase change solvents in CO<sub>2</sub> capture by NMR spectroscopy. *Chem. Eng. Sci.* 102, 378–386 <https://doi.org/10.1016/j.ces.2013.08.036>.
- Dash, S.K., Bandyopadhyay, S.S., 2016. Studies on the effect of addition of piperazine and sulfolane into aqueous solution of N-methyldiethanolamine for CO<sub>2</sub> capture and VLE modelling using eNRTL equation. *Int. J. Greenh. Gas Control* 44, 227–237 <https://doi.org/10.1016/j.ijggc.2015.11.007>.
- Daubert, T.E., Danner, R.P., Sibul, H.M., Stebbins, C.C., 1993. *Data Compilation of Pure Compound Properties*. DIPPR.
- Du, Y., Yuan, Y., Rochelle, G.T., 2016. Capacity and absorption rate of tertiary and hindered amines blended with piperazine for CO<sub>2</sub> capture. *Chem. Eng. Sci.* 155, 397–404 <https://doi.org/10.1016/j.ces.2016.08.017>.
- Dubois, L., 2013. *Etude de la capture du CO<sub>2</sub> en postcombustion par absorption dans des solvants aminés: application aux fumées issues de cimenteries*. PhD thesis. MONS University.
- Dubois, L., Thomas, D., 2018. Comparison of various configurations of the absorption-regeneration process using different solvents for the post-combustion CO<sub>2</sub> capture applied to cement plant flue gases. *Int. J. Greenh. Gas Control* 69, 20–35 <https://doi.org/10.1016/j.ijggc.2017.12.004>.
- Garcia, M., Knuutila, H.K., Gu, S., 2016. Thermodynamic modelling of unloaded and loaded N,N-diethylethanolamine solutions. *Green Energy Environ.* 1, 246–257 <https://doi.org/10.1016/j.gee.2016.11.003>.
- Garcia, M., Knuutila, H.K., Edwin, U., Gu, S., 2018. Influence of substitution of water by organic solvents in amine solutions on absorption of CO<sub>2</sub>. *Int. J. Greenh. Gas Control* 78, 286–305 <https://doi.org/10.1016/j.ijggc.2018.07.029>.
- Hartono, A., Saleem, F., Arshad, M.W., Usman, M., Svendsen, H.F., 2013. Binary and ternary VLE of the 2-(diethylamino)-ethanol (DEEA)/3-(methylamino)-propylamine (MAPA)/water system. *Chem. Eng. Sci.* 101, 401–411 <https://doi.org/10.1016/j.ces.2013.06.052>.
- Hessen, E.T., Haug-Warberg, T., Svendsen, H.F., 2010. The refined e-NRTL model applied to CO<sub>2</sub>-H<sub>2</sub>O-alkanolamine systems. *Chem. Eng. Sci.* 65, 3638–3648 <https://doi.org/10.1016/j.ces.2010.03.010>.
- Idem, R., Supap, T., Shi, H., Gelowitz, D., Ball, M., Campbell, C., Tontiwachwuthikul, P., 2015. Practical experience in post-combustion CO<sub>2</sub> capture using reactive solvents in large pilot and demonstration plants. *Int. J. Greenh. Gas Control* 40, 6–25 <https://doi.org/10.1016/j.ijggc.2015.06.005>.
- Khan, A.A., Halder, G.N., Saha, A.K., 2016. Comparing CO<sub>2</sub> removal characteristics of aqueous solutions of monoethanolamine, 2-amino-2-methyl-1-propanol, methyldiethanolamine and piperazine through absorption process. *Int. J. Greenh. Gas Control* 50, 179–189 <https://doi.org/10.1016/j.ijggc.2016.04.034>.
- Kim, I., 2009. *Heat of Reaction and VLE of Post Combustion CO<sub>2</sub> Absorbents*. PhD Thesis. Norwegian University of Science and Technology, Trondheim, Norway.
- Kim, I., Svendsen, H.F., Børresen, E., 2008. Ebulliometric determination of vapor-liquid equilibria for pure water, monoethanolamine, N-methyldiethanolamine, 3-(methylamino)-propylamine, and their binary and ternary solutions. *Chem. Eng.* 2521–2531.
- Laribi, S., Dubois, L., De Weireld, G., Thomas, D., 2019. Study of the post-combustion CO<sub>2</sub> capture process by absorption-regeneration using amine solvents applied to cement plant flue gases with high CO<sub>2</sub> contents. *Int. J. Greenh. Gas Control* 90, 102799 <https://doi.org/10.1016/j.ijggc.2019.102799>.
- le Bouhelec, E.B., Mougin, P., Barreau, A., Solimando, R., 2007. Rigorous modeling of the acid gas heat of absorption in alkanolamine solutions. *Energy Fuels* 21, 2044–2055 <https://doi.org/10.1021/ef0605706>.
- Li, H., Le Moullec, Y., Lu, J., Chen, J., Valle Marcos, J.C., Chen, G., Chopin, F., 2015. CO<sub>2</sub> solubility measurement and thermodynamic modeling for 1-methylpiperazine/water/CO<sub>2</sub>. *Fluid Phase Equilib.* 394, 118–128 <https://doi.org/10.1016/j.fluid.2015.03.021>.
- Lide, D.R., 2005. *CRC Handbook of Chemistry and Physics*. CRC Press, Taylor and Francis, Boca Raton FL [https://doi.org/10.1016/0165-9936\(91\)85111-4](https://doi.org/10.1016/0165-9936(91)85111-4).
- Liebenthal, U., Di, D., Pinto, D., Monteiro, J.G.M., Hallvard, F., Kather, A., 2013. Overall process analysis and optimisation for

- CO<sub>2</sub> capture from coal fired power plants based on phase change solvents forming two liquid phases. *Energy Procedia* 37, 1844–1854 <https://doi.org/10.1016/j.egypro.2013.06.064>.
- Luo, X., Chen, N., Liu, S., Rongwong, W., Idem, R.O., Paitoon, T., Liang, Z., 2016. Experiments and modeling of vapor-liquid equilibrium data in DEEA-CO<sub>2</sub>-H<sub>2</sub>O system. *Int. J. Greenh. Gas Control* 53, 160–168.
- Ma'mun, S., Svendsen, H.F., 2009. Solubility of N<sub>2</sub>O in aqueous monoethanolamine and 2-(2-aminoethyl-amino)ethanol solutions from 298 to 343 K. *Energy Procedia* 1, 837–843 <https://doi.org/10.1016/j.egypro.2009.01.111>.
- Mathonat, C., Oratoire, D., Maham, Y., Mather, A.E., Hepler, L.G., 1997. Excess molar enthalpies of (water + monoalkanolamine) mixtures at 298.15 K and 308.15 K. *J. Chem. Eng. Data*, 993–995.
- Mondal, B.K., Bandyopadhyay, S.S., Samanta, A.N., 2015. Vapor-liquid equilibrium measurement and ENRTL modeling of CO<sub>2</sub> absorption in aqueous hexamethylenediamine. *Fluid Phase Equilib.* 402, 102–112 <https://doi.org/10.1016/j.fluid.2015.05.033>.
- Monteiro, J., Svendsen, H.F., 2015. The N<sub>2</sub>O analogy in the CO<sub>2</sub> capture context: literature review and thermodynamic modelling considerations. *Chem. Eng. Sci.* 126, 455–470 <https://doi.org/10.1016/j.ces.2014.12.026>.
- Monteiro, J., Pinto, D., Zaidy, S., Hartono, A., Svendsen, H., 2013. VLE data and modelling of aqueous N,N-diethylethanolamine (DEEA) solutions. *Int. J. Greenh. Gas Control* 19, 432–440 <https://doi.org/10.1016/j.ijggc.2013.10.001>.
- Monteiro, J., Hussain, S., Majeed, H., Mba, E.O., Hartono, A., Knuutila, H., Svendsen, H.F., 2014. Kinetics of CO<sub>2</sub> absorption by aqueous 3-(methylamino) propylamine solutions: experimental results and modeling. *AIChE*, 1–12 <https://doi.org/10.1002/aic>.
- Monteiro, J., Knuutila, H., Nathalie, J.M.C., Elk, P., Versteeg, G., Svendsen, H.F., 2015a. Kinetics of CO<sub>2</sub>absorption by aqueous N,N-diethylethanolamine solutions: literature review, experimental results and modelling. *Chem. Eng. Sci.* 127, 1–12 <https://doi.org/10.1016/j.ces.2014.12.061>.
- Monteiro, J., Majeed, H., Knuutila, H., Svendsen, H.F., 2015b. Kinetics of CO<sub>2</sub> absorption in aqueous blends of N,N-diethylethanolamine (DEEA) and N-methyl-1,3-propane-diamine (MAPA). *Chem. Eng. Sci.* 129, 145–155.
- Perinu, C., Bernhardsen, I.M., Pinto, D.D.D., Knuutila, H.K., Jens, K., 2018. NMR Speciation of Aqueous MAPA, Tertiary Amines, and Their Blends in the Presence of CO<sub>2</sub>: Influence of pKa and Reaction Mechanisms. <https://doi.org/10.1021/acs.iecr.7b03795>.
- Perinu, C., Bernhardsen, I.M., Pinto, D.D.D., Knuutila, H.K., Jens, K.J., 2019. Aqueous MAPA, DEEA, and their blend as CO<sub>2</sub> absorbents: interrelationship between NMR speciation, pH, and heat of absorption data. *Ind. Eng. Chem. Res.* 58, 9781–9794 <https://doi.org/10.1021/acs.iecr.9b01437>.
- Pinto, D.D., 2014. CO<sub>2</sub> Capture Solvents: Modeling and Experimental Characterization. PhD Thesis. Norwegian University of Science and Technology, Trondheim, Norway.
- Pinto, D.D.D., Knuutila, H., Fytianos, G., Haugen, G., Mejell, T., Svendsen, H.F., 2014a. CO<sub>2</sub> post combustion capture with a phase change solvent. Pilot plant campaign. *Int. J. Greenh. Gas Control* 31, 153–164 <https://doi.org/10.1016/j.ijggc.2014.10.007>.
- Pinto, D.D.D., Zaidy, S.A.H., Hartono, A., Svendsen, H.F., 2014b. Evaluation of a phase change solvent for CO<sub>2</sub> capture: absorption and desorption tests. *Int. J. Greenh. Gas Control* 28, 318–327 <https://doi.org/10.1016/j.ijggc.2014.07.002>.
- Pinto, D.D.D., Johnsen, B., Awais, M., Svendsen, H.F., Knuutila, H.K., 2017. Viscosity measurements and modeling of loaded and unloaded aqueous solutions of MDEA, DMEA, DEEA and MAPA. *Chem. Eng. Sci.* 171, 340–350 <https://doi.org/10.1016/j.ces.2017.05.044>.
- Prausnitz, J.M., Lichtenhaler, R.N., Gomes de Azevedo, E., 1999. *Molecular Thermodynamics of Fluid-Phase Equilibria, third ed.* Prentice Hall International Series, New Jersey.
- Raynal, L., Alix, P., Bouillon, P.A., Gomez, A., Le Febvre De Nailly, M., Jacquin, M., Kittel, J., Di Lella, A., Mougin, P., Trapy, J., 2011. The DMX TM process: an original solution for lowering the cost of post-combustion carbon capture. *Energy Procedia* 4, 779–786 <https://doi.org/10.1016/j.egypro.2011.01.119>.
- Renon, H., Prausnitz, J.M., 1968. Local compositions in thermodynamic excess functions for liquid mixtures. *AIChE J.* 14, 135–144 <https://doi.org/10.1002/aic.690140124>.
- Sander, B., Fredenslund, A., Rasmussen, P., 1986. Calculation of vapour-liquid equilibria in mixed solvent/salt systems using an extended uniquac equation. *Chem. Eng. Sci.* 41, 1171–1183.
- Singh, P., Van Swaaij, W.P.M., Brilman, D.W.F., 2013. Energy efficient solvents for CO<sub>2</sub> absorption from flue gas: vapor liquid equilibrium and pilot plant study. *Energy Procedia* 37, 2021–2046 <https://doi.org/10.1016/j.egypro.2013.06.082>.
- Trolleboø, A.A., Saeeda, M., Hartono, A., Kimb, I., Svendsena, H.F., 2013. Vapour-liquid equilibrium for novel solvents for CO<sub>2</sub> post combustion capture. *Energy Procedia* 37, 2066–2075 <https://doi.org/10.1016/j.egypro.2013.06.085>.
- Xiao, M., Liu, H., Gao, H., Liang, Z., 2018. CO<sub>2</sub>absorption with aqueous tertiary amine solutions: equilibrium solubility and thermodynamic modeling. *J. Chem. Thermodyn.* 122, 170–182 <https://doi.org/10.1016/j.jct.2018.03.020>.
- Xu, Z., Wang, S., Qi, G., Trolleboø, A.A., Svendsen, H.F., 2014. Vapor liquid equilibria and heat of absorption of CO<sub>2</sub> in aqueous 2-(diethylamino)-ethanol solutions. *Int. J. Greenh. Gas Control* 29, 92–103 <https://doi.org/10.1016/j.ijggc.2010.04.005>.
- Zhang, Y., Chen, C., 2011. Thermodynamic modeling for CO<sub>2</sub> absorption in aqueous MDEA solution with electrolyte NRTL model. *Ind. Eng. Chem. Res.* 50, 163–175.
- Zhao, X., Smith, K.H., Simioni, M.A., Tao, W., Kentish, S.E., Fei, W., Stevens, G.W., 2011. Comparison of several packings for CO<sub>2</sub> chemical absorption in a packed column. *Int. J. Greenh. Gas Control* 5, 1163–1169 <https://doi.org/10.1016/j.ijggc.2011.07.006>.